Inorganic Chemistry

ARTICLE

pubs.acs.org/IC

Photoinduced Intramolecular Tryptophan Oxidation and Excited-State Behavior of $[Re(L\text{-}AA)(CO)_3(\alpha\text{-diimine})]^+$ (L = Pyridine or Imidazole, AA = Tryptophan, Tyrosine, Phenylalanine)

Ana María Blanco-Rodríguez,[†] Mike Towrie,[‡] J. Sýkora,[§] Stanislav Záliš,[§] and Antonín Vlček, Jr.*[,†,§]

[†]School of Biological and Chemical Sciences, Queen Mary University of London, Mile End Road, London E1 4NS, United Kingdom

[‡]Central Laser Facility, Research Complex at Harwell, STFC, Rutherford Appleton Laboratory, Harwell Oxford, Didcot, Oxfordshire OX11 0QX, United Kingdom

[§]J. Heyrovský Institute of Physical Chemistry, Academy of Sciences of the Czech Republic, Dolejškova 3, CZ-182 23 Prague, Czech Republic

Supporting Information

ABSTRACT: Re^I carbonyl-diimine complexes $[Re(L\text{-}AA)(CO)_3(N,N)]^+$ (N,N = bpy, phen) containing an aromatic amino acid (AA), phenylalanine (Phe), tyrosine (Tyr), or tryptophan (Trp), linked to Re by a pyridine-amido or imidazole-amido ligand L have been synthesized and their excited-state properties investigated by nanosecond time-resolved IR (TRIR) and emission spectroscopy. Near-UV optical excitation populates a $Re^I(CO)_3 \rightarrow N,N$ ^{3}MLCT excited state $*[Re^{II}(L\text{-}AA)(CO)_3(N,N^{\bullet-})]^+$. Decay to the ground state (50−300 ns lifetime) is the only excited-state deactivation process observed in the case of Phe and Tyr complexes, whereas the Trp-containing species undergo a Trp(indole)$\rightarrow$*Re^{II} electron transfer (ET) producing a charge-separated (CS) state, $[Re^I(L\text{-}Trp^{\bullet+})(CO)_3(N,N^{\bullet-})]^+$. The ET occurs with a 8−40 ns lifetime depending on L, N,N, and the solvent. The CS state is characterized by ν(CO) IR bands shifted to lower wavenumbers from their respective ground-state positions and two bands at 1278 and 1497 cm^{-1} tentatively attributed to $Trp^{\bullet+}$. The amido bridge is affected by both the MLCT excitation and the subsequent ET, manifested by the shifts and intensity changes of the amide-I IR band at about 1680 cm^{-1}. The CS state decays to the ground state by a $N,N^{\bullet-} \rightarrow Trp^{\bullet+}$ back-ET the rates of which are comparable to those of the forward ET, 30−60 ns. This study independently demonstrates that Trp can act as an electron-hopping intermediate in photodriven ET systems based on Re-labeled proteins and supramolecules. Photoinduced ET in Trp-containing Re complexes also can be used to generate $Trp^{\bullet+}$ and investigate its spectral properties and reactivity.

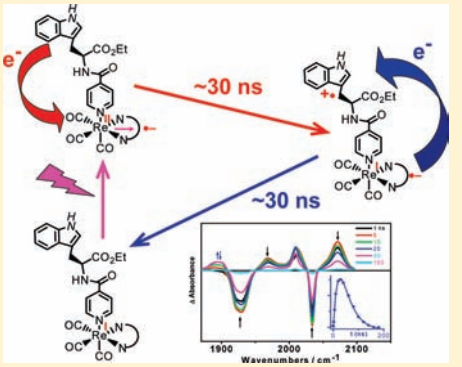

INTRODUCTION

Redox-active aromatic amino acids (AA) tryptophan (Trp) and tyrosine (Tyr) play an important role in biological electron transfer (ET), acting as redox-intermediates along electron-transfer pathways in proteins. Temporary Trp and Tyr oxidation splits long tunneling pathways into shorter steps. Resulting sequential tunneling (hopping) mechanism can accomplish very fast charge separation over long distances, often longer than 2 nm. Out of many examples, we may single out the enzyme DNA photolyase, where an arrangement of three tryptophans mediates a 30 ps electron transfer across 1.5 nm.[1−3] Class 1 ribonucleotide reductase (RNR) provides another example,[4,5] incorporating a chain of tyrosines and tryptophans to transfer charge from an iron-tyrosyl cofactor over two protein subunits to an active site 3.5 nm apart. Whereas Trp mostly acts as an electron (hole) transfer mediator, Tyr oxidation is often coupled with proton transfer, as is the case of RNR, photosystem II,[5,6] and many other enzymes.

Kinetics and mechanism of biological electron transfer reactions often are investigated by labeling proteins with metal−diimine chromophores that become strong oxidants upon optical excitation (Re^I) or photochemical oxidation by an external quencher (Ru^{II}, Os^{II}).[7] Very fast excitation of the metallolabel triggers electron-transfer from the protein, whose rate and intermediates are investigated by following spectroscopic features of the metallolabel and/or protein functional groups as a function of time. This approach is well-suited to obtain kinetics data on long-range electron transfer,[7−9] as well as to investigate the electron hopping mechanism involving tryptophan[7,10,11] or proton-coupled electron transfer reactions of tyrosine.[12] For several reasons, Re^I carbonyl-diimine complexes[13,14] are favored ET phototriggers: (i) they can be easily appended to biomolecules, (ii) their excited states are strongly oxidizing and long-lived (thus avoiding the necessity to use external quenchers), and (iii) their excited-state lifetime and the redox potential can be finely tuned by variations of the diimine and/or the axial ligand. For example, a functional "photoRNR" has

Received: February 6, 2011
Published: June 08, 2011

been constructed,[12] in which a fluorinated tyrosine group (F_nTyr) of a [Re(CN)(CO)$_3$(bpy-F_nTyr)] complex occupies the site of one of the natural Tyr residues of the RNR enzyme. Photoexcitation of the Re(CN)(CO)$_3$(bpy) chromophore generates F_nTyr$^{\bullet}$ by a F_nTyr→*Re ET coupled with F_nTyr$^{+\bullet}$ deprotonation, initiates radical hopping through the protein molecule, and accomplishes high turnover deoxynucleotide formation, while kinetics and mechanistic information are unraveled through spectroscopic detection of the F_nTyr$^{\bullet}$ intermediate.[12]

Recently, a dramatic acceleration of a long-range (∼2 nm) ET from a Cu^{I} center in the *Pseudomonas aeruginosa* protein azurin to excited Re^{I}(CO)$_3$(4,7-dimethylphenanthroline)$^{+}$ chromophore appended to the protein close to a Trp residue was demonstrated.[10] No ET occurs when Tyr, lysine, or Phe occupies the Trp site. Kinetics analysis revealed several Trp→*Re ET steps whose rates range from hundreds of femtoseconds to units of nanoseconds.[10,11] Thus, the Cu^{I}→*Re ET is accelerated by splitting the 2 nm pathway into much shorter Trp→*Re and Cu^{I}→Trp$^{+\bullet}$ steps, over which electron tunneling occurs with ∼500 ps and 30 ns lifetimes, respectively.[10,11] Detailed spectroscopic and computational study of this system has revealed that the peptide segment containing the Re label and the proximal Trp residue behaves as a single redox-active unit with $\pi-\pi$ interaction between the Trp(indole) ring and the phenanthroline ligand.[11]

The propensity of Re^{I} chromophores to photooxidize aromatic amino acids in biomolecules (as well as supramolecular constructs[15]) presents an interesting mechanistic challenge and commands investigations of the photobehavior of Re^{I} carbonyl-diimine complexes containing aromatic amino acids. So far, Tyr→*Re ET and its coupling with a proton transfer (PCET) were studied upon MLCT excitation of [Re(PPh$_2$Ph-Tyr)-(CO)$_3$(phen)]$^{+}$ and [Re(CN)(CO)$_3$(bpy-F_nTyr)] (phen =1, 10-phenanthroline, bpy =2,2′-bipyridine).[12,16,17] A theoretical analysis of this reaction in an aqueous phosphate buffer solution has identified a close interaction between the tyrosine −OH group and the proton acceptor HPO_4^{3-} as the prerequisite for fast Tyr oxidation.[18] A detailed PCET mechanistic understanding has been obtained on Ru^{II}−bipyridine complexes with covalently attached Tyr.[19−21] Using a Ru^{II}−bpy assembly with appended Trp has shown that Trp photooxidation at acidic or neutral pH occurs as an ET process, producing Trp$^{+\bullet}$, followed by a relatively slow (130 ns at pH = 8) deprotonation to Trp$^{\bullet}$.[20] Another stream of research has produced a series of Re^{I} carbonyl-phenanthroline complexes of Trp analogues [Re(py-indole)-(CO)$_3$(R-phen)]$^{+}$, where indole is covalently attached to a pyridine ligand through an amide link and aliphatic chains of variable lengths.[22−24] These complexes are very promising luminescent labels and probes for indole-binding proteins.[22−25]

Aiming at a better understanding of aromatic amino acid oxidation by electronically excited Re^{I} chromophores, we have prepared a series of complexes [Re(L-AA)(CO)$_3$(N,N)]$^{+}$ (L = py or imidazole, N,N = bpy, phen, AA = Trp, Tyr, Phe; Figure 1) and investigated their excited-state behavior in several aprotic solvents using emission and picosecond−nanosecond time-resolved IR spectroscopy (TRIR). This approach allowed us to characterize the excited states and redox intermediates involved and to determine the ET kinetics. We have found that excitation of the Re^{I}(CO)$_3$(N,N) chromophore triggers an intramolecular nanosecond Trp oxidation, followed by a back-electron-transfer of a comparable rate. The relatively slow forward ET rates can be understood in view of the lack of a direct contact between the indole group and the polypyridine ligand.

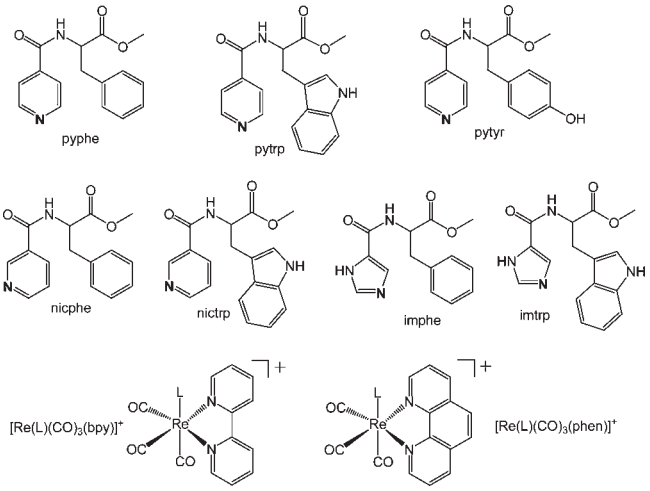

Figure 1. Pyridine and imidazole amino acid ligands L-AA and their abbreviations. Donor atoms are indicated in bold. Bottom row: schematic structures of the Re complexes. (Actual ligand structures are most likely trans with respect to the peptide bond; see Figure 2.)

EXPERIMENTAL SECTION

Materials. Starting materials were obtained from Aldrich and used as received. All measurements were performed in solvents of spectroscopic purity.

4-(Amino acid)pyridine Ligands (pyaa). Isonicotinic acid chloride hydrochloride (1 g, 5.62 mmol) was suspended in DCM (40 mL), and triethylamine (∼3 mL) was added until the solid dissolved. The amino acid methyl ester (hydrochloride salt in the case of Trp and Phe) (1.14 mol equiv) was added, turning the solution orange. The reaction mixture was stirred at room temperature for 10 min. The resulting precipitate ($Et_3N\cdot HCl$) was filtered off and the DCM solution was washed with water (4 × 50 mL). The solvent was removed by rotary evaporation to give the desired ligands in yields of 50−60%

3-(4-Hydroxyphenyl)-2-[(pyridine-4-carbonyl)amino]propionic Acid Methyl Ester (pytyr). White solid. ^{1}H NMR (DMSO, 270 MHz): 2.93 (1H, dd, ^3J = 9.4 Hz, ^2J = 14 Hz, CH methylene), 3.06 (1H, dd, ^3J = 5.5 Hz, ^2J = 14 Hz CH methylene), 3.75 (3H, s, CH_3), 4.82 (1H, m, CH), 6.9 (2H, d, ^3J = 8.5 Hz, phenol), 7.5 (2H, d, ^3J = 8.5 Hz, phenol), 7.69 (2H, dd, ^3J = 6.2 Hz, ^5J = 1.7 Hz, py), 8.73 (2H, dd, ^3J = 6.2 Hz, ^5J = 1.7 Hz, py), 9.09 (1H, d, ^3J = 7.9 Hz, NH), 9.21 (1H, s, OH). ^{13}C NMR (CD_3OD, 67.9 MHz): 172.1 (CO), 166.6 (CO), 156.2 (C, phenol), 149.6 (CH × 2, py), 142.1 (C, phenol), 129.9 (CH × 2, phenol), 127.5 (C, py), 121.7 (CH × 2, py), 115.0 (CH × 2, phenol), 54.8 (CH), 51.6 (OCH_3), 36.1 (CH_2). MS (ES) *m*/*z*: calcd for $C_{16}H_{16}N_2O_4$ (M^+ + Na) 323.1008, found 323.0998.

3-(1*H*-Indol-3-yl)-2-[(pyridine-4-carbonyl)amino]propionic acid methyl ester (pytrp). Yellow/brown oil. ^{1}H NMR (DMSO, 270 MHz): 3.23 (1H, dd, ^3J = 5 Hz, CH methylene), 3.31 (1H, dd, ^3J = 7.4 Hz, CH methylene), 3.64 (3H, s, Me), 4.72 (1H, m, CH), 7.01 (2H, m, indole), 7.21 (1H, s, indole), 7.35 (1H, d, ^3J = 7.9 Hz, indole), 7.57 (1H, d, ^3J = 7.9 Hz, indole), 7.71 (2H, dd, ^3J = 6.2 Hz, ^5J = 1.5 Hz, py), 8.71 (2H, dd, ^3J = 6.2 Hz, ^5J = 1.5 Hz, py), 9.15 (1H, d, ^3J = 7.4 Hz, NH), 10.85 (1H, s, NH). ^{13}C NMR (CD_3OD, 67.9 MHz): 172.4 (CO), 166.6 (CO), 149.5 (CH × 2, py), 142.1 (C, py), 136.7 (C, indole), 127.4 (C, indole), 123.1 (CH, indole), 121.7 (CH × 2, py), 121.2 (CH, indole), 118.6 (CH, indole), 117.8 (CH, indole), 111.1 (CH, indole) 109.6 (C, indole), 54.3 (CH), 51.5 (OCH_3), 26.9 (CH_2). MS ES *m*/*z*: calcd for $C_{18}H_{17}N_3O_3$ (M^+ + Na) 346.1168, found 346.1158.

dx.doi.org/10.1021/ic200252z |*Inorg. Chem.* 2011, 50, 6122–6134

3-Phenyl-2-[(pyridine-4-carbonyl)amino]propionic Acid Methyl Ester (pyphe). Brown oil. ^{1}H NMR ($CDCl_3$, 270 MHz): 3.20 (1H, dd, ^3J = 9.9 Hz, ^2J = 14 Hz, CH methylene), 3.27 (1H, dd, ^3J = 5.5 Hz, ^2J = 14 Hz CH methylene), 3.77 (3H, s, Me), 4.75 (1H, m, CH), 6.75 (1H, s, NH), 7.27 (5H, m, phenyl CH), 7.53 (2H, dd, ^3J = 6.2 Hz, ^5J = 1.7 Hz, py), 8.70 (2H, dd, ^3J = 6.2 Hz, ^5J = 1.7 Hz, py). ^{13}C NMR (CD_3OD, 67.9 MHz): 171.9 (CO), 166.5 (CO), 149.6 (CH × 2, py), 142.1 (C, py), 137.0 (C, phenyl), 128.8 (CH × 2, phenyl), 128.3 (CH × 2, phenyl), 126.6 (CH, phenyl), 121.6 (CH × 2, py), 54.6 (CH), 51.6 (OCH_3), 36.8 (CH_2). MS ES m/z: calcd for $C_{16}H_{16}N_2O_3$ (M^+ + Na) 307.1059, found 307.1051.

3-(Amino acid)pyridine Ligands (nicaa). Nicotinic acid chloride hydrochloride (1 g, 5.62 mmol) was suspended in DCM (40 mL), and triethylamine (~3 mL) was added until the solid dissolved. The amino acid methyl ester hydrochloride salt (1.14 mol equiv) was added, turning the solution orange. The reaction mixture was stirred at room temperature for 10 min. The resulting precipitate ($Et_3N\cdot HCl$) was filtered off and the DCM solution was washed with water (4 × 50 mL) The mixture was washed successively with water, 0.1 N aqueous hydrochloric acid, water, 5% aqueous sodium bicarbonate solution, and water; dried over sodium sulfate; and evaporated. Then, 100 mL of ether was added and the solution was evaporated again. The product was obtained as yellow, hygroscopic crystals in ~50−60% yield.

3-(1*H*-Indol-3-yl)-2-[(pyridine-3-carbonyl)amino]propionic Acid Methyl Ester (nictrp). ^{1}H NMR ($CDCl_3$, 270 MHz): 3.23 (1H, dd, ^3J = 5 Hz, CH methylene), 3.31 (1H, dd, ^3J = 7.4 Hz, CH methylene), 3.62 (3H, s, Me), 5.09 (1H, m, CH), 7.01 (2H, m, indole), 7.21 (1H, s, indole), 7.49 (1H, d, ^3J = 7.7 Hz, indole), 7.57 (1H, d, ^3J = 7.4 Hz, indole), 7.85 (2H, d, ^3J = 7.7 Hz, py), 8.43 (2H, d, ^3J = 4.7 Hz, py), 8.82 (1H, s, py), 9.48 (1H, s, NH). ^{13}C NMR ($CDCl_3$, 67.9 MHz): 172.6 (CO), 165.9 (CO), 152.0 (CH, py), 148.2 (C, py), 136.5 (C, indole), 135.3 (CH, py), 129.7 (CH, py), 127.4 (C, indole), 123.5 (CH, indole), 123.2 (CH, py), 122.1 (CH, indole), 119.5 (CH, indole), 118.4 (CH, indole), 111.8 (CH, indole) 109.5 (C, indole), 54.0 (CH), 52.6 (OCH_3), 27.5 (CH_2). MS ES m/z: calcd for $C_{18}H_{18}N_3O_3^+$ (M^+ + H) 324.1348, found 324.1340.

3-Phenyl-2-[(pyridine-3-carbonyl)amino]propionic Acid Methyl Ester (nicphe). ^{1}H NMR ($CDCl_3$, 270 MHz): 3.0 (1H, dd, ^3J = 7.7 Hz, ^2J = 14 Hz, CH methylene), 3.07 (1H, dd, ^3J = 5.5 Hz, ^2J = 14 Hz CH methylene), 3.52 (3H, s, Me), 4.88 (1H, m, CH), 6.75 (1H, s, NH), 7.27 (5H, m, phenyl CH), 7.81 (2H, d, ^3J = 7.7 Hz, py), 8.43 (2H, d, ^3J = 4.7 Hz, py), 8.82 (1H, s, py). ^{13}C NMR ($CDCl_3$, 67.9 MHz): 172.1 (CO), 165.7 (CO), 152.0 (CH, py), 148.3 (C, py), 136.3 (C, phenyl), 135.2 (CH, py), 129.7 (C, py) 129.1 (CH × 2, phenyl), 128.5 (CH × 2, phenyl), 127.0 (CH, phenyl), 123.3 (CH, py), 54.0 (CH), 52.3 (OCH_3), 37.5 (CH_2). MS ES m/z: calcd for $C_{16}H_{17}N_2O_3^+$ (M^+ + H) 285.1239, found 285.1241

4-(Amino acid)imidazole Ligands (imaa). 4-Imidazolecarboxylic acid (0.3 g, 2.6 mmol) and LiOH (1.1 mol equiv) were dissolved in MeOH (~40 mL). A few drops of water were added until the solids went into solution. The solvent was removed to yield a white powder (lithium imidazole carboxylate salt) that was used for the next step without further purification. The powder was dissolved with the amino acid methyl ester hydrochloride salt (0.67 mol equiv) and PyBOP (1 mol equiv) in dry DMF (20 mL). The reaction mixture was stirred for 12 h at room temperature. The DMF was removed under reduced pressure, and the resulting oil was dissolved in DCM and washed with water (4 × 50 mL). The organic layer was dried over sodium sulfate and evaporated. The resulting solid was purified by means of flash chromatography (Si column and a DCM:MeOH:Et_2NH 94:5:1 solvent system) to yield the desired ligand in 36−40% yield.

2-[(1*H*-Imidazole-4-carbonyl)amino]-3-(1*H*-indol-3-yl)propionic Acid Methyl Ester (imtrp). White crystals. ^{13}C NMR (CD_3OD, 67.9 MHz): 172.7 (CO), 163.3 (CO), 136.7 (C, indole), 136.2 (CH, im), 134.4 (C, im), 127.4 (C, indole), 123.4 (CH, indole), 121.3 (CH, indole), 120.9 (CH, im), 118.7 (CH, indole), 118.0 (CH, indole), 111.2 (CH, indole) 109.1 (C, indole), 53.2 (CH), 51.6 (OCH_3), 27.4 (CH_2). MS ES m/z: calcd for $C_{16}H_{17}N_4O_3^+$ (M^+ + H) 313.1301, found 313.1285.

2-[(1*H*-Imidazole-4-carbonyl)amino]-3-phenylpropionic Acid Methyl Ester (imphe). White/yellow solid. ^{13}C NMR ($CDCl_3$, 67.9 MHz): 172.2 (CO), 163.2 (CO), 136.1 (C, phenyl), 136 (CH, im), 135.0 (C, im) 129.2 (CH × 2, phenyl), 128.7 (CH × 2, phenyl), 127.2 (CH, phenyl), 120.3 (CH, im), 53.4 (CH), 52.5 (OCH_3), 38.1 (CH_2). MS ES m/z: calcd for $C_{14}H_{16}N_3O_3^+$ (M^+ + H) 274.1192, found 274.1182.

[Re(L)(CO)$_3$(N,N)]PF$_6$ (L = pyaa, nicaa, imaa; N,N = bpy, phen). A modified published procedure[26] was used: [$Re(CF_3SO_3)(CO)_3(NN)$] (0.171 g, 0.299 mmol) was refluxed with the pyaa ligand (1 mol equiv) in MeOH for 3 h. Upon cooling, the solvent was removed and the resulting product was redissolved in the minimum amount of MeOH. A saturated solution of NH_4PF_6 in MeOH (~3 mL) was added to the reaction mixture and the product was precipitated as a yellow solid by adding water, filtered, and air-dried. The compounds were purified by precipitation from DCM with diethyl ether. The pure product is a pale yellow solid (yield ~70%).

[Re(pytyr)(CO)$_3$(bpy)]PF$_6$. ^{1}H NMR (CD_2Cl_2, 400 MHz): 2.92 (1H, dd, ^3J = 6.8 Hz, ^2J = 14 Hz CH methylene), 3. 04 (1H, dd, ^3J = 5.3 Hz, ^2J = 14 Hz CH methylene), 3.63 (3H, s, Me), 4.74 (1H, m, CH), 5.4 (1H, s, OH), 6.59 (2H, d, ^3J = 8.3 Hz, phenol), 6.65 (1H, d, ^3J = 7.6 Hz, NH), 6.84 (2H, d, ^3J = 8.3 Hz, phenol), 7.43 (2H, dd, ^3J = 6.6 Hz, ^5J = 1.5 Hz, py), 7.71 (2H, m, bpy), 8.17 (2H, dd, ^3J = 6.6 Hz, ^5J = 1.5 Hz, py), 8.19 (2H, m, bpy), 8.27 (2H, d, ^3J = 8.1 Hz, bpy), 9.08 (2H, d, ^3J = 5.1 Hz, bpy). ^{13}C NMR (CD_2Cl_2, 100.6 MHz): 195.8 (CO), 191.4 (CO), 171.6 (CO), 163.4 (CO), 156.0 (C × 2, bpy), 155.6 (C, phenol), 153.5 (CH × 2, bpy), 152.7 (CH × 2, py), 144.7 (C, phenol), 141.8 (CH × 2, bpy), 130.7 (CH × 2, phenol), 129.5 (CH × 2, bpy), 127.8 (C, py), 125.3 (CH × 2, bpy), 124.9 (CH × 2, py), 115.9 (CH × 2, phenol) 54.6 (CH), 52.8 (OCH_3), 37.8 (CH_2). MS ES m/z: calcd for $C_{29}H_{24}N_4O_7Re^+$ (M^+) 727.1202, found 727.1189. IR (CH_2Cl_2): ν(CO) = 2037 (s), 1938 (br) cm^{-1}.

[Re(pytrp)(CO)$_3$(bpy)]PF$_6$. ^{1}H NMR (CD_2Cl_2, 400 MHz): 3.21 (2H, d, ^3J = 5.7 Hz, CH_2), 3.55 (3H, s, Me), 4.77 (1H, m, CH), 6.80 (1H, d, J = 7.8 Hz, NH), 6.87 (1H, t, ^3J = 7.1 Hz, indole), 6.97 (1H, s, indole), 6.98 (1H, t, indole), 7.19 (1H, d, ^3J = 8.1 Hz, indole), 7.31 (1H, d, ^3J = 7.9 Hz, indole), 7.37 (2H, dd, ^3J = 6.7 Hz, ^5J = 1.4 Hz, py), 7.63 (2H, m, bpy), 8.06 (2H, m, bpy), 8.11 (2H, m, ^3J = 8.1 Hz, bpy), 8.14 (2H, dd, ^3J = 6.7 Hz, ^5J = 1.5 Hz, py), 8.60 (1H, s, NH), 9.03 (2H, d, ^3J = 5.4 Hz, bpy). ^{13}C NMR (CD_2Cl_2, 100.4 MHz): 195.7 (CO), 191.4 (CO), 172.0 (CO), 163.5 (CO), 155.8 (C × 2, bpy), 153.6 (CH × 2, bpy), 152.8 (CH × 2, py), 144.4 (C, indole), 141.6 (CH × 2, bpy), 136.7 (C, indole), 129.5 (CH × 2, bpy), 127.5 (C, py), 125.1 (CH × 2, bpy), 124.8 (CH × 2, py), 124.4 (CH, indole), 122.4 (CH, indole), 119.7 (CH, indole), 118.5 (CH, indole), 112.0 (CH, indole), 109.2 (C, indole), 54.6 (CH), 52.8 (OCH_3), 37.8 (CH_2). MS ES m/z: calcd for $C_{31}H_{25}N_5O_6Re^+$ (M^+) 750.1362, found 750.1323. IR (CH_2Cl_2): ν(CO) = 2037 (s), 1937 (br) cm^{-1}.

[Re(pytrp)(CO)$_3$(phen)]PF$_6$. ^{13}C NMR (CD_2Cl_2, 100.4 MHz): 196.7 (CO), 192.8 (CO), 173.6 (CO), 166.3 (CO), 156.3 (CH × 2, py), 154.2 (CH × 2, phen), 151.3 (C × 2, phen), 148.0 (C, indole), 146.0 (C × 2, phen), 142.1 (CH × 2, phen), 138.4 (C, indole), 133.1 (C, py), 129.8 (CH × 2, phen), 128.9 (CH × 2, phen), 125.8 (CH × 2, py), 124.8 (CH, indole), 122.8 (CH, indole), 120.1 (CH, indole), 119.4 (CH, indole), 112.8 (CH, indole), 111.0 (C, indole), 56.1 (CH), 53.3 (OCH_3), 28.5 (CH_2). MS ES m/z: calcd for $C_{34}H_{25}N_4O_6Re^+$ (M^+) 774.1362, found 774.1337. IR (MeCN): ν(CO) = 2037 (s), 1933 (br) cm^{-1}.

[Re(pyphe)(CO)$_3$(bpy)]PF$_6$. ^{1}H NMR (CD_2Cl_2, 400 MHz): 3.09 (1H, dd, ^3J = 7.4 Hz, ^2J = 14 Hz CH methylene), 3.23 (1H, dd, ^3J = 5.5 Hz,

^2J = 14 Hz, CH methylene), 3.72 (3H, s, Me), 4.87 (1H, m, J = 5.6 Hz, CH), 6.84 (1H, d, J = 7.8 Hz, NH), 7.15 (2H, d, J = 6.7 Hz, phenyl), 7.25 (3H, m, phenyl), 7.57 (2H, dd, ^3J = 6.7 Hz, ^5J = 1.5 Hz, py), 7.82 (2H, m, J = 5.4 Hz, bpy), 8.27 (2H, dd, ^3J = 6.7 Hz, ^5J = 1.5 Hz, py), 8.31 (2H, m, J = 8.2 Hz, bpy), 8.40 (2H, d, ^3J = 8.2 Hz, bpy), 9.18 (2H, d, ^3J = 5.5 Hz, bpy). ^{13}C NMR (CD_2Cl_2, 100.6 MHz): 195.8 (CO), 191.4 (CO), 171.5 (CO), 163.5 (CO), 156.0 (C, bpy), 153.4 (CH × 2, bpy), 152.7 (CH × 2, py), 144.7 (C, phenyl), 141.8 (CH × 2, bpy), 136.4 (CH, phenyl), 129.5 (CH × 2, bpy), 129.4 (CH × 2, phenyl), 129.0 (CH × 2, phenyl), 127.4 (CH, py), 125.3 (CH × 2, bpy), 125.0 (CH × 2, py), 54.6 (CH), 52.8 (OCH_3), 37.8 (CH_2). MS ES *m/z*: calcd for $C_{29}H_{24}N_4O_6Re^+$ (M^+) 711.1253, found 711.1213. IR (CH_2Cl_2): ν(CO) = 2037 (s), 1936 (br) cm^{-1}.

[Re(nictrp)(CO)$_3$(bpy)]PF$_6$. ^{13}C NMR (CD_3CN, 67.9 MHz): 195.7 (CO), 191.4 (CO), 172.6 (CO), 165.9 (CO), 152.9 (C × 2, bpy), 151.8 (CH × 2, bpy), 151.3 (CH, py), 150.2 (CH, py), 148.3 (C, py), 140.9 (CH × 2, bpy), 137.8 (CH, py), 136.1 (C, indole), 132.1 (CH, py), 128.5 (CH × 2, bpy), 127.8 (C, indole), 124.4 (CH × 2, bpy), 123.1 (CH, indole), 121.4 (CH, indole), 118.8 (CH, indole), 118.3 (CH, indole), 111.3 (CH, indole), 109.5 (C, indole), 53.6 (CH), 51.7 (OCH_3), 30.7 (CH_2). MS ES *m/z*: calcd for $C_{31}H_{25}N_5O_6Re^+$ (M^+) 750.1362, found 750.1338. IR (MeCN): ν(CO) = 2037 (s), 1932 (br) cm^{-1}.

[Re(nicphe)(CO)$_3$(bpy)]PF$_6$. ^{13}C NMR ($CDCl_3$, 67.9 MHz): 195.2 (CO), 191.3 (CO), 172.1 (CO), 163.4 (CO), 155.4 (C × 2, bpy), 153.1 (CH × 2, bpy), 151.1 (CH, py), 149.1 (C, py), 141.5 (CH × 2, bpy), 137.8 (CH, py), 136.4 (C, phenyl), 132.5 (C, py), 129.9 (CH × 2, bpy), 129.2 (CH × 2, phenyl), 128.6 (CH × 2, phenyl), 127.9 (CH, phenyl), 125.5 (CH × 2, bpy), 122.8 (CH, py), 54.5 (CH), 52.5 (OCH_3), 37.5 (CH_2). MS ES *m/z*: calcd for $C_{29}H_{24}N_4O_6Re^+$ (M^+) 711.1253, found 711.1218. IR (MeCN): ν(CO) = 2037 (s), 1933 (br) cm^{-1}.

[Re(nictrp)(CO)$_3$(phen)]PF$_6$. ^{13}C NMR (MeOD, 67.9 MHz): 196.3 (CO), 192.3 (CO), 173.5 (CO), 165.5 (CO), 155.6 (CH, py), 152.7 (C × 2, phen), 151.9 (CH, py), 147.5 (CH × 2, phen), 141.9 (CH × 2, phen), 139.5 (CH, py), 138.0 (CH, py), 137.2 (C, indole), 133.7 (C × 2, phen), 132.6 (CH, py), 129.5 (CH × 2, phen), 128.6 (CH × 2, phen), 127.7 (C, indole), 124.6 (CH, indole), 121.6 (CH, indole), 119.9 (CH, indole), 119.1 (CH, indole), 112.6 (CH, indole), 110.9 (C, indole), 55.7 (CH), 53.0 (OCH_3), 28.2 (CH_2). MS ES *m/z*: calcd for $C_{33}H_{25}N_5O_6Re^+$ (M^+) 774.1362, found 774.1329. IR (MeCN): ν(CO) = 2037 (s), 1934 (br) cm^{-1}.

[Re(nicphe)(CO)$_3$(phen)]PF$_6$. ^{13}C NMR ($CDCl_3$, 67.9 MHz): 195.2 (CO), 191.3 (CO), 172.1 (CO), 163.4 (CO), 156.2 (CH, py), 154.2 (C × 2, phen), 150.8 (CH, py), 146.4 (CH × 2, phen), 140.6 (CH × 2, phen), 137.8 (CH, py), 136.2 (C, phenyl), 132.1 (C × 2, phen), 131.3 (C, py), 129.2 (CH × 2, phenyl), 128.6 (CH × 2, phenyl), 127.6 (CH × 2, phen), 127.1(CH, phenyl), 124.4 (CH × 2, phen), 122.9 (CH, py), 54.3 (CH), 52.5 (OCH_3), 37.6 (CH_2). MS ES *m/z*: calcd for $C_{29}H_{24}N_4O_6Re^+$ (M^+) 735.1253, found: 735.1214. IR (MeCN): ν(CO) = 2037 (s), 1932 (br) cm^{-1}.

[Re(imtrp)(CO)$_3$(bpy)]PF$_6$. ^{13}C NMR (CD_3CN, 67.9 MHz): 196.7 (CO), 192.7 (CO), 171.5 (CO), 162.7 (CO), 156.9 (C, im), 155.4 (C × 2, bpy), 153.4 (CH × 2, bpy), 140.6 (CH × 2, bpy), 140.2 (CH, im), 136.1 (C, indole), 129.1 (CH, im), 128.2 (CH × 2, bpy), 126.9 (C, indole), 124.4 (CH × 2, bpy), 123.3 (CH, indole), 121.3 (CH, indole), 118.7 (CH, indole), 117.9 (CH, indole), 111.1 (CH, indole), 109.2 (C, indole), 53.0 (CH), 51.6 (OCH_3), 26.7 (CH_2). MS ES *m/z*: calcd for $C_{29}H_{24}N_6O_6Re$ (M^+) 739.1315, found 739.1274. IR (CH_2Cl_2): ν(CO) = 2034 (s), 1928 (br) cm^{-1}.

[Re(imphe)(CO)$_3$(bpy)]PF$_6$. ^{13}C NMR (CD_3CN, 67.9 MHz): 196.7 (CO), 192.7 (CO), 171.5 (CO), 162.7 (CO), 157.1 (C, im), 155.2 (C × 2, bpy), 153.4 (CH × 2, bpy), 142.7 (CH, im), 141.6 (CH × 2, bpy), 136.8 (C, phenyl), 130.7 (CH × 2, bpy), 130.2 (CH, im), 129.9 (CH × 2, phenyl), 128.3 (CH × 2, phenyl), 126.3 (CH, phenyl), 124.4 (CH × 2, bpy), 55.2 (CH), 53.2 (OCH_3), 38.1 (CH_2). MS ES *m/z*: calcd for $C_{27}H_{23}N_5O_6Re$ (M^+) 700.1206, found 700.1209. IR (CH_2Cl_2): ν(CO) = 2033 (s), 1930 (br) cm^{-1}.

Physical Measurements. NMR spectra were recorded on JEOL EX 270 (^{1}H, 270 MHz; ^{13}C, 67.9 MHz) or Bruker AMX400 (^{1}H, 400 MHz; ^{13}C[^{1}H], 100.61 MHz) spectrometers. ^{1}H NOESY spectra were obtained with a 600 MHz Bruker AV600 instrument. High-resolution electrospray mass spectrometry was performed by Kings College, University of London, on an Apex III system.

UV−vis and FTIR absorption spectra were measured with HP8453 and PE1720X spectrometers, respectively. Emission spectra were obtained on Jobin Yvon (Horiba) FluoroMax-3 and Fluorolog-3 instruments using 405 nm excitation. Emission lifetime and time-resolved anisotropy measurements were performed using time-correlated single-photon counting (TCSPC) on an IBH 5000 U instrument equipped with a cooled Hamamatsu R3809U-50 microchannel plate photomultiplier. The samples (aerated solutions) were excited at 405 nm with a diode laser (IBH NanoLED-07, fwhm 80 ps, 500 kHz repetition rate).

Time-resolved IR measurements in the ν(CO) spectral region were obtained with the PIRATE instrument.[27−29] In short, for measurements in the 0−2000 ps time domain, the sample solution was excited (pumped) at 400 nm, using frequency-doubled pulses from a Ti:sapphire laser of ∼150 fs duration (fwhm) and ca. 3 μJ energy, focused at an area ∼200 μm in diameter. TRIR spectra were probed with spectrally broad IR pulses (∼150 fs, ∼200 cm^{-1}) obtained by difference-frequency generation from the same Ti:sapphire laser. In the nanosecond range, sample excitation was performed with 355 nm, ∼0.7 ns fwhm, ∼3 μJ laser pulses generated by an actively Q-switched AOT-YVO-20QSP/MOPA Nd:vanadate diode-pumped microlaser that was electronically synchronized with the femtosecond probe system.[30] The ULTRA instrument[31] has been used for TRIR experiments in the fingerprint region. A titanium sapphire laser/regenerative amplifier (Thales) produces ∼50 fs pulses at a 10 kHz repetition rate. The laser output is split in two parts, one of which is frequency-doubled to 400 nm and used as a pump beam. The second pumps a TOPAS OPA, yielding signal and idler beams that are difference frequency mixed to generate ∼400 cm^{-1} broad mid-IR probe pulses. The mid-IR probe spectrum is recorded at a given time delay using two 128-element HgCdTe detectors (Infrared Associates). The sample solutions (aerated, 1−5 mM [Re]) were flowed through a 0.1 mm CaF_2 plate cell that was at the same time scanned-rastered across the irradiated area in two dimensions to prevent laser heating and decomposition of the sample. FTIR spectra measured before and after the experiment demonstrated sample stability. All spectral and kinetics fitting procedures were performed using MicroCal Origin 7.1.

Quantum Chemical Calculations. The structures of different conformations of [Re(imtrp)(CO)$_3$(bpy)]$^+$ complex were calculated by density functional theory (DFT) methods using the Gaussian 09[32] program package. DFT calculations employed Perdew, Burke, Ernzerhof[33,34] (PBE0) and long-range corrected CAM-B3LYP[35] hybrid functionals. Polarized triple-ζ basis sets 6-311g(d)[36] were used for H, C, N, and O atoms, together with quasirelativistic effective core pseudopotentials and the corresponding optimized set of basis functions[37,38] for Re. Geometry optimizations were followed by vibrational analysis in order to characterize stationary states. The solvent (MeCN) was described by the polarizable calculation model (PCM).[39]

RESULTS

Synthesis and Structures. The amino acid-bearing pyridine or imidazole ligands (L-AA, Figure 1) were made by reacting the pyridinecarbonyl chlorides or imidazolecarboxylic acid with the corresponding amino acid methyl ester. The Re complexes were prepared following the well-established[26] route to cationic Re carbonyl diimine complexes, by reacting the ligand L with

dx.doi.org/10.1021/ic200252z |Inorg. Chem. 2011, 50, 6122–6134

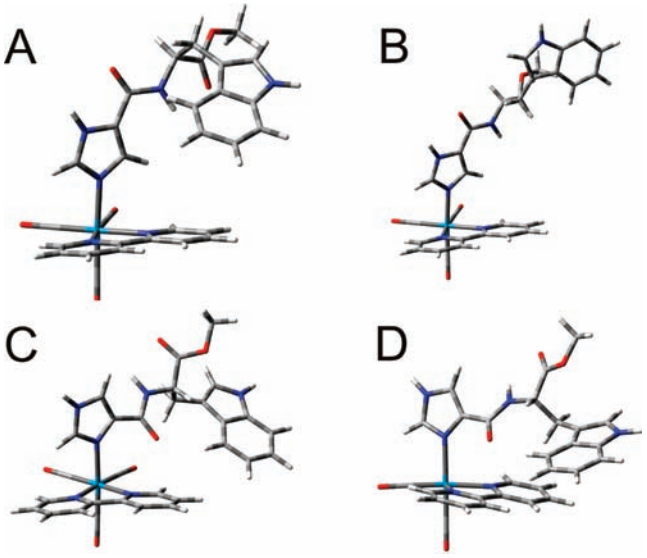

Figure 2. DFT-optimized structures of selected $[Re(imtrp)(CO)_3(bpy)]^+$ conformers in MeCN. Calculated Gibbs free energies relative to the most stable structure A: B, 0.054 eV; C, 0.128 eV; D, 0.182 eV.

$[Re(OTf)(CO)_3(N,N)]$, which was generated from $[Re(Cl)(CO)_3(N,N)]$ using Ag(OTf). The complexes show typical UV−vis absorption spectra consisting (for N,N = bpy) of an IL band at 320 nm and a shoulder due to Re→N,N MLCT transition(s) at ∼340 nm for the pyridine-based complexes, or a maximum at ∼353 nm for the imidazole-containing species (Supportimg Information, Figure S1). IR spectra of all the complexes are virtually identical, showing a sharp band at 2033−2037 cm^{-1} and a broad band at 1927−1933 cm^{-1} assigned[40] to the in-phase A′(1) and quasidegenerate A′(2) + A″ ν(CO) vibrations, respectively.

Relevant to ET reactivity are possible contacts and π−π stacking between the amino acid aromatic side chain and the diimine ligand. Simple molecular models show that such interactions are hardly possible for the pyaa and nicaa ligands. This conclusion is supported by a ^{1}H NOESY (t_m = 350 ms, 303 K, CD_2Cl_2) spectrum of $[Re(pytrp)(CO)_3(bpy)]^+$ that does not show any cross-peaks between the indole and bpy hydrogen atoms. On the other hand, it shows cross-peaks between the amide and pyridine-C3 as well as between the pyridine-C2 and bpy-C6 H-atoms. It follows that the peptide group is in a trans configuration and the pytrp indole is oriented away from the $Re(CO)_3(bpy)$ chromophore. $[Re(imtrp)(CO)_3(bpy)]^+$ can exist in two isomeric forms. Figure 2 shows two characteristic stable structures for each isomer calculated by DFT. The structure A was calculated to have the lowest energy. The imidazole plane is oriented perpendicularly to the symmetry plane, i.e., bisecting the angles between the equatorial OC−Re−N angles, and the closest distance between indole and the bpy ligand is 4.53 Å, while the respective molecular planes contain quite a large angle. The second rotamer of structure A (the imidazole plane coincidental with the symmetry plane, not shown) is only about 0.02 eV higher in energy. Energetically very close is the conformer B, where the indole group points away from both the Re center and the bpy ligand. The lowest energy structure corresponding to less-stable second isomer is the structure C, with the imidazole plane oriented perpendicularly to the symmetry plane and imidazole pointing away from the bpy ligand. The conformer D, with the im plane parallel to the symmetry plane and the indole group close to the bpy ligand, lies at higher energy. With relatively low ΔG° differences, it is well possible that several conformers of both isomers are present simultaneously in the solution.

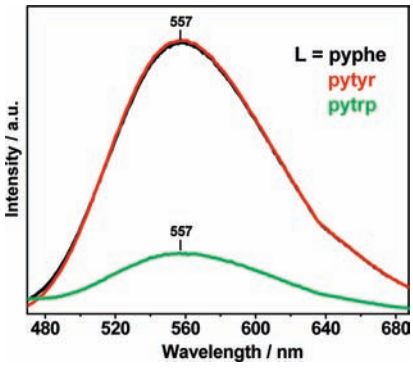

Figure 3. Emission spectra of $[Re(pyaa)(CO)_3(bpy)]^+$ in MeCN at 21 °C. Concentrations of the sample solutions were adjusted to give identical absorbance of 0.1 at the 405 nm excitation wavelength. Spectra are not corrected for the detector response.

Emission Spectroscopy. All investigated complexes in MeCN solutions show broad unstructured emission with a maximum at 550−585 nm (N,N = bpy) and 546−549 nm (N,N = phen), as is expected[14,26,40,41] for a ^{3}MLCT state of Re^I carbonyl-diimines. Emission energies depend little on the appended aa group in the case of pyaa complexes, while a small blue-shift was observed on going from nicphe to nictrp (3−11 nm) and from imphe to imtrp (19 nm). Emission spectra and band-maximum wavelengths are summarized in Figures 3 and S2 (Supportimg Information). $[Re(pyphe)(CO)_3(bpy)]^+$ and $[Re(pytyr)(CO)_3(bpy)]^+$ emission occur with identical intensities, whereas emission from $[Re(pytrp)(CO)_3(bpy)]^+$ is ca. 4.3 times weaker (Figure 3). Intensity quenching was observed for all investigated Trp-containing complexes.

Emission lifetimes of pyphe, pytyr, and nicphe complexes (Supportimg Information, Figure S3) depend only slightly on L (Table 1). Phen complexes have longer-lived emission than bpy, 270−300 and 140−150 ns, respectively. A biexponential decay with the principal lifetime of 50 ns and a minor 2 ns component was found for $[Re(imphe)(CO)_3(bpy)]^+$. The amplitude of the 2 ns decay sharply decreases with increasing detection wavelength, turning to a small early time rise at long wavelengths; see Figure S4 (Supporting Information). This behavior suggests that the 2 ns decay arises from structural and/or solvational relaxation.[42]

Emission of Trp complexes decays bi- or triexponentially (Table 1). The major emission decay component is significantly faster than for the Phe analogues. Since Trp-localized excited states lie high above ^{3}MLCT and the complexes are photostable, we can exclude energy transfer and bond breaking, leaving Trp(indole)→Re^{II} ET as the likely quenching mechanism. The short minor decay component (2−3 ns) has a wavelength-dependent amplitude (Supporting Information, Figure S4) and is again attributed to relaxation processes. The other minor (<10%) component has a lifetime only a little shorter than that of the corresponding Phe-containing species and is assigned to an unreactive conformer. To detect the Re reduction product and prove the ET mechanism, we have resorted to structure-sensitive TRIR spectroscopy. (Note that visible time-resolved absorption would not be a suitable technique in this case because of a large

Table 1. Emission and TRIR Lifetime Data (ns) Measured in Air-Saturated MeCN Solutions at 21 °C[a]

	emission lifetimes[b]		TRIR lifetimes			
	τ (major)	τ (minor)	CS rise	CS decay	MLCT decay	bleach recovery
$[Re(pytrp)(bpy)]^+$	27.0 (95)	214 (5)	19.5 ± 2	40 ± 6	29.3 ± 0.7	42.9 ± 0.7
	30.0[c]	242[c]				
$[Re(pytyr)(bpy)]^+$	147	–	–	–	109 ± 3	117.6 ± 0.1
	300[c]					
$[Re(pyphe)(bpy)]^+$	144	–	–	–	129 ± 3	127 ± 3
	296[c]					
$[Re(pytrp)(phen)]^+$	26.9 (77)	2.0 (14)	14.2 ± 0.5	56 ± 2	29 ± 2	54 ± 2
		221 (10)				
$[Re(pyphe)(phen)]^+$	281	–	–	–	233 ± 13	255 ± 11
$[Re(nictrp)(bpy)]^+$	8.8 (93)	114 (7)	6.3 ± 0.5	32 ± 3	9.3 ± 0.3[d]	29.6 ± 1[d]
$[Re(nicphe)(bpy)]^+$	144	–	–	–	125 ± 6	141 ± 10
$[Re(nictrp)(phen)]^+$	7.3[d]	–	5.5 ± 0.8	33 ± 4	5.7 ± 2[d]	30 ± 6[d]
$[Re(nicphe)(phen)]^+$	301	–	–	–	212 ± 4	237 ± 3
$[Re(imtrp)(bpy)]^+$	22.0 (87)	3.0 (13)	16 ± 3	160 ± 1	19 ± 1	19 ± 3 (76)
						144 ± 63 (14)
$[Re(imphe)(bpy)]^+$	49.8 (86)	2.3 (14)	–	–	54 ± 5	49 ± 2

[a] Percentage amplitudes in parentheses. Emission decay kinetics were measured at the wavelength corresponding to the emission band maximum. [b] accuracy ±0.1−1.0%. [c] Measured in degassed solutions. [d] Additional low-amplitude long-lifetime component present.

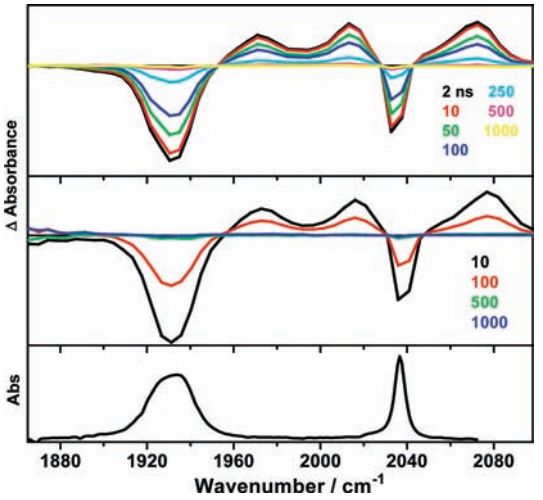

Figure 4. TRIR spectra of $[Re(pyphe)(CO)_3(bpy)]^+$ (top) and $[Re(pytyr)(CO)_3(bpy)]^+$ (middle) in MeCN solutions. Spectra were measured at the specified time delays (in ns) after 355 nm, 0.7 ns excitation. The experimental points are separated by 4−5 cm^{-1}. Bottom: Ground-state FTIR spectrum of $[Re(nictrp)(CO)_3(bpy)]^+$ in MeCN.

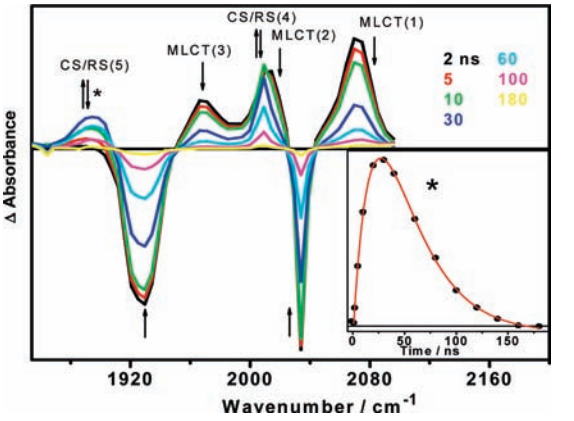

Figure 5. TRIR spectrum of $[Re(pytrp)(CO)_3(bpy)]^+$ in MeCN, following 355 nm, 0.7 ns excitation. Experimental points are separated by 4−5 cm^{-1}. Arrows indicate rise and decay of the transients. Inset: kinetics profile taken from band 5, as marked by the asterisk.

overlap of Trp^+ and $Trp^•$ absorption, 550−600 and 520 nm, respectively,[20] with that of the excited and reduced states of Re diimine complexes.[43−46])

Time-Resolved Infrared Spectroscopy. Nanosecond difference TRIR spectra (Figure 4) of $[Re(pyphe)(CO)_3(bpy)]^+$ and $[Re(pytyr)(CO)_3(bpy)]^+$ show two negative bands (bleaches) due to a depleted ground-state population and three positive bands at 2073, 2013, and 1971 cm^{-1}, corresponding[40] to the A′(1), A′(2), and A″ excited-state vibrations, respectively. Very similar spectra were obtained for other $[Re(L\text{-}Phe/L\text{-}Tyr)(CO)_3(N,N)]^+$ complexes. The shift of the A′(1) vibration by ca. 37 cm^{-1} (N,N = bpy) and 26 cm^{-1} (N,N = phen) to higher energy and splitting of the quasidegenerate A′(2) + A″ vibrations upon excitation are characteristic IR features of ^{3}MLCT excited states.[13,28,40,47−51] TRIR bands decay with kinetics that are, within the experimental accuracy, comparable to the principal kinetics component of the emission decay (Table 1). TRIR spectra measured in the ps range show the typical[29,52−57] relaxation-related dynamic upshift that is completed in the first ∼30 ps.

Nanosecond TRIR spectra of $[Re(pytrp)(CO)_3(bpy)]^+$ (Figure 5) and other L-Trp complexes (Figure 6) point to a more complicated excited-state behavior. The ^{3}MLCT IR bands (denoted 1−3 in Figure 5) are formed virtually instantaneously upon excitation. Their decay is faster than for Phe and Tyr complexes and accompanied by a simultaneous rise of new features 4 and 5 at ∼2010 and ∼1895 cm^{-1}, respectively, whose intensities first increase and then decay (Figure 5, inset). The two intermediate

dx.doi.org/10.1021/ic200252z |Inorg. Chem. 2011, 50, 6122–6134

bands 4 and 5 are shifted to lower energies from the corresponding bleach bands by 25 and 36 cm^{-1}, respectively. Such a spectral pattern is typical for reduced $[Re^{I}(L\text{-}N)(CO)_3(bpy^{\bullet-}/phen^{\bullet-})]$ complexes, where L-*N* is a nitrogen-coordinated ligand such as MeCN, picoline, or pyridine, which have been generated either electrochemically[58−60] or photochemically.[49,59,61] Accordingly, the transient bands 4 and 5 are attributed to a charge-separated (CS) state $[Re^{I}(L\text{-}Trp^{\bullet+})(CO)_3(bpy^{\bullet-})]^{+}$ and/or a reduced state (RS) $[Re^{I}(L\text{-}Trp)(CO)_3(bpy^{\bullet-})]$, which cannot be distinguished by IR spectra. The ET product(s) then decay back to the ground state, manifested in TRIR by the decay of the bands 4 and 5 and a concomitant bleach recovery. Figure 6 documents the qualitatively similar behavior of all the investigated Trp complexes. In the case of $[Re(imtrp)(CO)_3(bpy)]^{+}$, the CS bands at 1895 and 2010 cm^{-1} are weaker and the 1895 cm^{-1} feature shifts to higher energies with time, probably due to the formation of a small amount of a persistent photoproduct that is still visible in the TRIR spectrum measured 2 ms after excitation. No CS signal was seen in picosecond TRIR spectra measured in the 1−1000 ps range, excluding any subnanosecond ET reactivity.

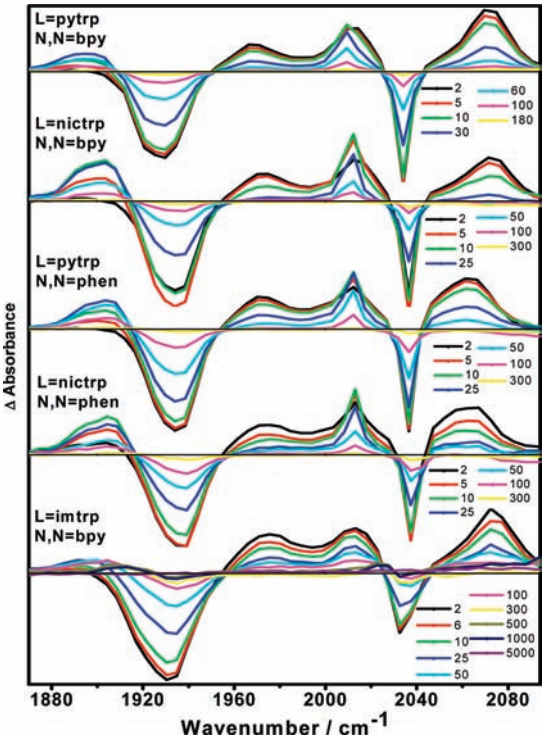

Figure 6. TRIR spectra of $[Re(L\text{-}Trp)(CO)_3(N,N)]^{+}$ in MeCN solutions, following 355 nm, 0.7 ns excitation. Time delays in nanoseconds. Experimental points are separated by 4−5 cm^{-1}.

TRIR detection of the CS and/or RS proves the ET mechanism of the MLCT excited-state quenching of the Trp complexes (Scheme 1). Optical excitation produces the ^{3}MLCT state $^{*}[Re^{II}(L\text{-}Trp)(CO)_3(N,N^{\bullet-})]^{+}$ that undergoes either intermolecular or intramolecular Trp(indole)→$^{*}Re^{II}$ ET shown in Scheme 1 in blue and red, respectively. The photocycle is completed by $N,N^{\bullet-}$→Trp($indole^{\bullet+}$) back-electron-transfer, BET. Further confirmation of this mechanism and information on electronic delocalization and structural changes of the pytrp ligand were obtained by TRIR spectra measured on $[Re(pytrp)(CO)_3(bpy)]^{+}$ in the fingerprint region.

The ground-state FTIR spectrum of $[Re(pytrp)(CO)_3(bpy)]^{+}$ (Figure 7) shows the C═O stretch of the ester group at 1744 cm^{-1} in DCM (1747 cm^{-1} in MeCN) and the amide-I band (C═O stretching/N−H bending vibration) at 1678 cm^{-1} in DCM (1676 cm^{-1} in MeCN). The bands at 1604 (1606 cm^{-1} in MeCN), 1493, 1472, and 1447 cm^{-1} correspond[62] to bpy-localized vibrations, while the strong band at 1521 cm^{-1} most likely belongs to overlapping Trp amide-II and indole vibrations. The origins of the weaker bands at 1358, 1418, and 1457 cm^{-1} are not clear.

The TRIR spectrum of the MLCT state, measured at 1 ns after excitation (Figure 8, blue), exhibits a weak bleach of the amide-I band, together with an overlapping transient feature whose maximum is shifted by ca. +9 cm^{-1} to 1685 cm^{-1}. The CS-state spectrum was obtained at 60 ns (Figure 8, red). The amide-I band is bleached but without a discernible transient, suggesting that the energy is the same as in the ground state but the molar

Scheme 1. Excited-State Electron Transfer Reactivity of $[Re^{I}(L\text{-}Trp)(CO)_3(N,N)]^{+}$: (left, blue) Bimolecular Quenching Involving Intermolecular ET and (right, red) Intramolecular ET Pathway

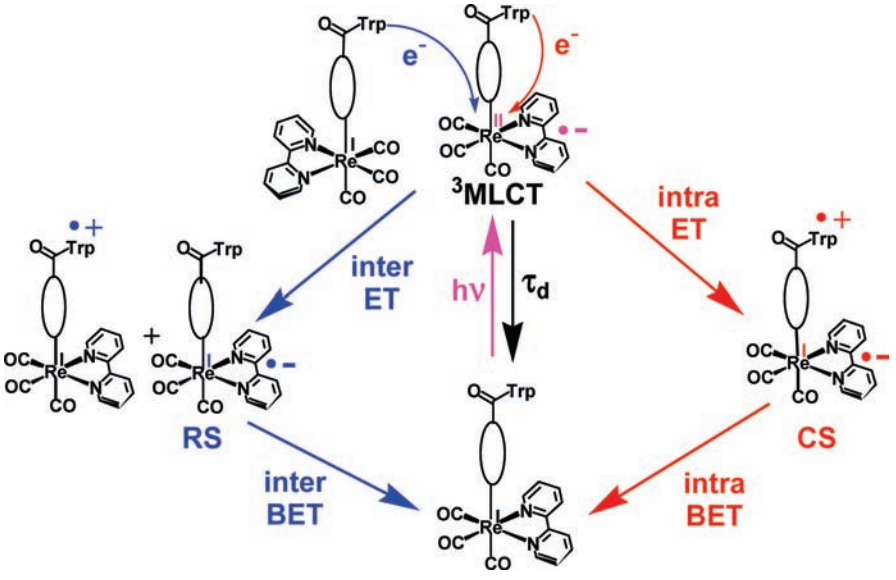

dx.doi.org/10.1021/ic200252z |*Inorg. Chem.* 2011, 50, 6122–6134

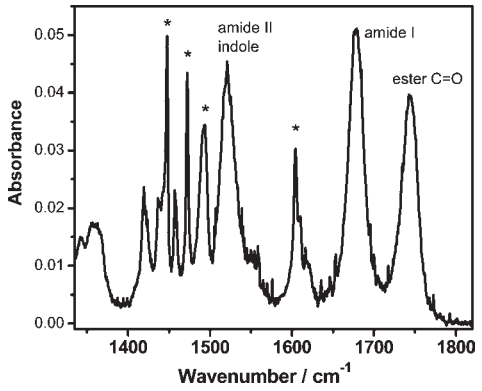

Figure 7. Ground-state FTIR spectrum of $[Re(pytrp)(CO)_3(bpy)]^+$ in DCM in the fingerprint region. The band maxima occur at 1358, 1418, 1447, 1457, 1472, 1493, 1521, 1604, 1678, and 1744 cm^{-1}. The asterisks denote bpy bands.[62]

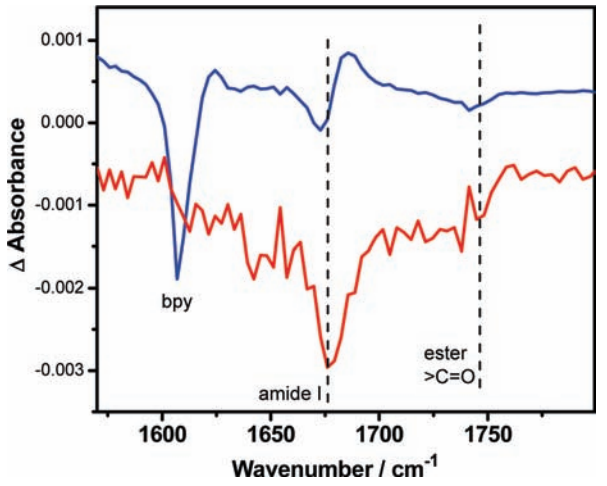

Figure 8. TRIR spectra of $[Re^I(pytrp)(CO)_3(N,N)]^+$ in the 1570−1800 cm^{-1} range measured at 1 ns (blue, attributed to MLCT) and 60 ns (red, attributed to CS) after 355 nm, 0.7 ns excitation. Experimental points are separated by ~3 cm^{-1}. (Measured in MeCN using the ULTRA TRIR instrument.[31])

absorptivity is smaller. The ester C═O band is bleached very little upon both MLCT excitation and the following ET, implying that the ester group is almost unaffected. (A slightly more intense bleach was observed for the CS state in DCM.)

The 1606 cm^{-1} bpy band is strongly bleached in the MLCT TRIR spectrum (Figure 8), probably due to a drop in intensity upon excitation, rather than a band shift.[62] (The weak signal at ~1627 cm^{-1} appears to be a high-energy wing of a weak broad overlapping transient.) The 1606 cm^{-1} bleach intensity decreases with time during the first 30 ns, becoming unobservable after about 40 ns in MeCN, whereas it remains weakly apparent in DCM. This behavior can be explained by assuming that the overlapping (positive) transient band gains intensity and narrows on going from the MLCT to the CS state, possibly due to a weak $Trp^{\bullet+}\cdots bpy^{\bullet-}$ interaction in the latter.

The bpy bands at 1315, 1448, and 1472 cm^{-1} are strongly bleached in the MLCT TRIR spectrum measured at 1 ns (Figure 9, blue). The most prominent MLCT transient band occurs at 1441 cm^{-1}, together with weaker bands at 1359 and 1426 cm^{-1}, plus a broad absorption that overlaps with the

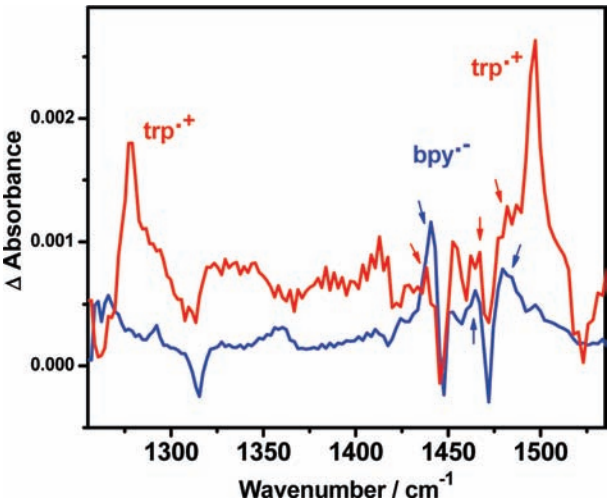

Figure 9. TRIR spectra of $[Re^I(pytrp)(CO)_3(N,N)]^+$ in the region of aromatic-ring vibrations measured at 1 ns (blue, attributed to MLCT) and 50 ns (red, attributed to CS) after 355 nm, 0.7 ns excitation. Experimental points are separated by 2−3 cm^{-1}. Typical $bpy^{\bullet-}$ transient bands are denoted by arrows. (Measured in DCM using the ULTRA TRIR instrument.[31])

1472 cm^{-1} bleach. These transient features are comparable to those observed[62] in the step-scan TRIR spectrum of MLCT-excited $[Re(4\text{-ethylpyridine})(CO)_3(bpy)]^+$, supporting our assignment. The spectrum measured at 50 ns (Figure 9, red), when the CS state is the predominant species in the solution, shows two strong bands at 1278 and 1497 cm^{-1} that are attributable to $Trp^{\bullet+}$, in particular to vibrations of the oxidized indole$^{\bullet+}$. In addition, the Trp-specific band at 1521 cm^{-1} is bleached in the CS but not in the MLCT spectrum. The bleached bpy bands and corresponding $bpy^{\bullet-}$ transients are still present in the CS state. Altogether, the TRIR spectra confirm the ^{3}CS formulation as $[Re(pytyr^{\bullet+})(CO)_3(bpy^{\bullet-})]^+$ and the mechanism proposed in Scheme 1: The bleached bpy bands and $bpy^{\bullet-}$ transients are present immediately after excitation as well as after the Trp→*Re^{II} ET, whereas the bleached Trp band and $Trp^{\bullet+}$ transients emerge only upon the CS formation.

Electron Transfer Kinetics. The rate constants k_{ET} of the Trp(indole)→Re^{II} excited-state ET were calculated from the MLCT excited-state lifetimes τ_d of the Trp complexes using the formula

$$k_{ET} = 1/\tau_d - 1/\tau_0 \quad (1)$$

τ_0 is the inherent MLCT lifetime, for which the lifetimes of the corresponding unreactive Phe complexes were used. The lifetime values were determined from the decay of the emission intensity as well as of the A′(1) and A″ TRIR bands 1 and 3. In the case of multiexponential decay kinetics, the lifetime of the major decay component was used (Table 1).

The BET rate constants were determined from the biexponential rise and decay kinetics of the TRIR CS/RS band 5 at ~1895 cm^{-1} (Figure 5, inset). The data were fitted to eq 2:

$$I(5) = A_1 e^{-t/\tau_d} + A_2 e^{-t/\tau_{BET}} + A_0 \quad (2)$$

One of the time constants (τ_d) can be identified with the MLCT lifetime, while the second is attributed to the back-electron-transfer; $\tau_{BET} = k_{BET}^{-1}$.

dx.doi.org/10.1021/ic200252z |Inorg. Chem. 2011, 50, 6122–6134

Table 2. Rate Constants (s^{-1}) of Photoinduced Electron Transfer Reactions in $[Re(L\text{-}Trp)(CO)_3(N,N)]^+$ Complexes in MeCN at 21 °C

	k_{ET}			
	emission[a]	TRIR MLCT[b]	TRIR CS/CR[c]	k_{BET}: TRIR CS/CR[c]
$[Re(pytrp)(bpy)]^+$	3.0×10^7	2.6×10^7	4.4×10^7	2.5×10^7
$[Re(pytrp)(phen)]^+$	3.4×10^7	3.0×10^7	6.6×10^7	1.8×10^7
$[Re(nictrp)(bpy)]^+$	1.1×10^8	1.0×10^8	1.5×10^8	3.1×10^7
$[Re(nictrp)(phen)]^+$	1.3×10^8	1.7×10^8	1.8×10^8	3.0×10^7
$[Re(imtrp)(bpy)]^+$	2.5×10^7	3.4×10^7	4.4×10^{7d}	6.3×10^{6d}

[a] Determined from emission decay and eq 1, with ±1% accuracy. A small systematic error may arise from the presence of relaxation kinetics components that affect decay fits. [b] From TRIR-measured decay of MLCT IR bands and eq 1, with an accuracy between ±8 and ±15%. [c] From biexponential fits of the CS/RS band at 1890 cm^{-1} (eq 2); k_{ET} determined from eq 1; $k_{BET} = \tau_{BET}^{-1}$. Accuracy was between ±8 and ±15%. [d] Estimate, with an accuracy of ±34%.

Table 3. Rate Constants (s^{-1}) of Photoinduced Electron Transfer Reactions in $[Re(pytrp)(CO)_3(bpy)]^+$ in Various Solvents at 21 °C[a]

		MeCN	DMF	DCM	THF
k_{ET}/s^{-1}		2.6×10^7	4.3×10^7	6.1×10^7	7.5×10^7
k_{BET}/s^{-1}	k_{BET1}	2.5×10^7	1.7×10^7	2.5×10^{7c}	4.1×10^7
	k_{BET2}	–	–	3.7×10^{6c}	1.8×10^6
$1/\varepsilon_{op} - 1/\varepsilon_s$[b]		0.529	0.463	0.383	0.375
viscosity/cP[d]		0.35	0.92	0.45	0.55

[a] Accuracy from ±8% to ±14%. [b] From ref 63. [c] ±30%. [d] From ref 64.

The rate constants are summarized in Table 2. The k_{ET} values determined from emission and TRIR MLCT decay lifetimes are well-comparable, whereas those obtained from the biexponential fits of the weaker CS/CR band (third column) are subjected to a larger error. The values obtained from the CS/CR band of $[Re(imtrp)(CO)_3(bpy)]^+$ are only rough estimates, since the measured intensity changes are affected by the gradual band shift to higher energies, which indicates a chemical reaction of the CS (or RS) state.

TRIR spectra and ET kinetics of $[Re(pytrp)(CO)_3(bpy)]^+$ were investigated in a series of solvents with different dielectric properties: MeCN, *N*,*N*-dimethylformamide (DMF), CH_2Cl_2 (DCM), and tetrahydrofuran (THF). The excited-state behavior is qualitatively the same as described above for MeCN, although a biexponential CS/CR decay was observed in DCM and THF. The rate constants and lifetimes are summarized in Tables 3 and S1 (Supporting Information), respectively. Small band-shape changes and upshift usually accompany the CS/RS band 5 decay, and a small amount of a CS/RS product persists at 500 ns. The back ET is slightly slower than the forward ET in all solvents except MeCN, leading to larger CS yields [compare Figures 5 and S5 (Supporting Information) showing TRIR spectra obtained in MeCN and DMF, respectively].

Intramolecular or Intermolecular Electron Transfer? As shown in Scheme 1, left, the tryptophan unit in one $[Re(pytrp)(CO)_3(bpy)]^+$ molecule can quench the excited state of another molecule. Bimolecular ET quenching by Trp(indole) is documented in Figure 10, which shows TRIR spectra of

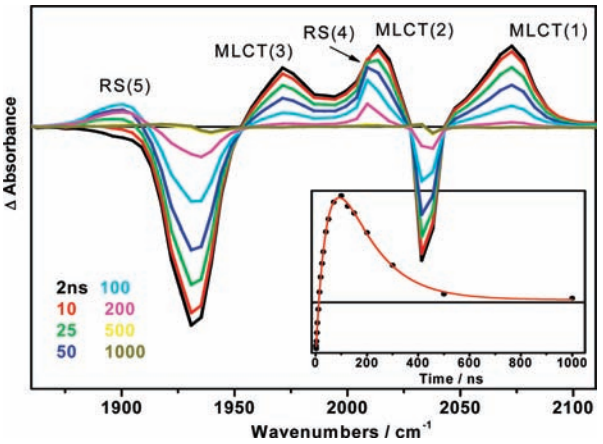

Figure 10. TRIR spectra of 2.0×10^{-3} M $[Re(pyphe)(CO)_3(bpy)]^+$ and 2.0×10^{-3} tryptophan methyl ester in MeCN, following 355 nm, 0.7 ns excitation. Time delays in nanoseconds. Peaks are labeled in accordance with Figure 5. Inset: kinetic profile of the RS(5) band peak intensity. The experimental points are separated by 4−5 cm^{-1}.

Table 4. TRIR Kinetics Data for 2.02×10^{-3} M $[Re(pyphe)(CO)_3(bpy)]^+$ and Different Molar Equivalents of Tryptophan Methyl Ester

[Trp]/M	0	2.02×10^{-3}	3.14×10^{-3}
RS rise/ns	–	50 ± 3	45 ± 4
RS decay/ns	–	135 ± 10	126 ± 15
MLCT decay/ns	129 ± 3	70 ± 2	55 ± 2
bleach recovery/ns	124 ± 3	99 ± 1	96 ± 5
$k_{ET(app)}/s^{-1}$ MLCT[a]	–	6.5×10^6	1.0×10^7
$k_{2,ET}/M^{-1}s^{-1}$[b]	–	3.2×10^9	3.2×10^9
$k_{BET(app)}/s^{-1}$[c]	–	7.4×10^6	7.9×10^6

[a] Calculated using eq 1 from MLCT lifetimes measured in the presence and absence of the quencher. [b] $k_{2,ET} = k_{ET(app)}/[Trp]$. [c] Calculated from the RS decay (eq 2).

$[Re(pyphe)(CO)_3(bpy)]^+$ measured in the presence of a molar equivalent of a tryptophan methyl ester, Me-Trp. The features due to the redox state (RS) $[Re^I(pyphe)(CO)_3(bpy^{\bullet-})]$ occur at 1890 and 2009 cm^{-1}, undistinguishable from the IR bands of the CS/RS state $[Re^I(pytrp^{\bullet+})(CO)_3(bpy^{\bullet-})]^+$ shown in Figure 5.

The redox state is formed by a bimolecular excited-state ET:

$$*[Re^I(pyphe)(CO)_3(bpy)]^+ + \text{Me-Trp} \xrightarrow{k_{2,ET}} [Re^I(pyphe)(CO)_3(bpy^{\bullet-})] + \text{Me-Trp}^{\bullet+} \quad (3)$$

followed by the corresponding back-ET. The TRIR-determined kinetics parameters (Table 4) show that the bimolecular quenching is nearly diffusion-controlled. Nevertheless, the pseudo-monomolecular rate constant $k_{ET(app)}$ measured at typical TRIR concentrations is 5−3 times smaller than the k_{ET} obtained for $[Re^I(pytrp)(CO)_3(bpy)]^+$, while BET is 6 times slower. These observations indicate that the ET kinetics reported above for $[Re^I(pytrp)(CO)_3(bpy)]^+$ are mostly attributable to intramolecular processes.

To assess the role of bimolecular ET in the excited-state behavior of $[Re^I(pytrp)(CO)_3(bpy)]^+$ more quantitatively, we

dx.doi.org/10.1021/ic200252z |*Inorg. Chem.* 2011, 50, 6122–6134

Table 5. Concentration Dependence of $[Re(pytrp)(CO)_3(bpy)]^+$ TRIR Kinetics in MeCN

concentration/M	3.7×10^{-3}	2.7×10^{-3}	9.6×10^{-4}	4.2×10^{-4}
MLCT/ns, τ_d	28.2 ± 0.4	29.7 ± 0.4	31.3 ± 0.4	31.9 ± 0.8
CS/RS decay/ns	48 ± 4	46 ± 2	36 ± 5	46 ± 7
bleach recovery/ns	51 ± 2	52 ± 2	53 ± 2	47 ± 1
k_{ET}/s^{-1} [a]	2.8×10^7	2.6×10^7	2.4×10^7	2.4×10^7
k_{BET}/s^{-1} [b]	2.1×10^7	2.2×10^7	2.8×10^7	2.2×10^7

[a] Calculated using eq 1 where τ_d is the MLCT lifetime of $[Re(pytrp)(CO)_3(bpy)]^+$ at given concentration and τ_0 is the $[Re(pyphe)(CO)_3(bpy)]^+$ MLCT lifetime (129 ns). [b] Calculated from the CS/RS decay (eq 2).

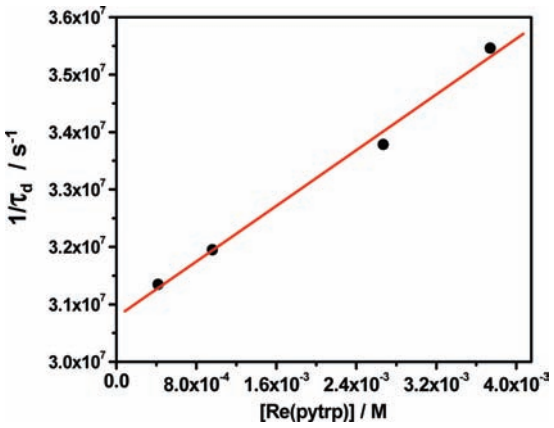

Figure 11. Concentration dependence of the reciprocal $[Re(pytrp)(CO)_3(bpy)]^+$ MLCT lifetime in MeCN. The linear fit (1.21×10^9 M^{-1} s^{-1} slope and 3.08×10^7 s^{-1} intercept) is shown in red.

have investigated the dependence of the TRIR kinetics on the $[Re(pytrp)(CO)_3(bpy)]^+$ concentration (Table 5). The data show that the MLCT lifetime slightly increases with decreasing concentration while k_{ET} decreases, albeit in a narrow range.

In the simultaneous presence of inter- and intramolecular quenching (Scheme 1), the MLCT lifetime τ_d will depend on the concentration [Re(pytrp)] according to eq 4:

$$\frac{1}{\tau_d} = \frac{1}{\tau_0} + k_{ET}^{intra} + k_Q[Re(pyrtrp)] \quad (4)$$

k_{ET}^{intra} is the rate constant of the intramolecular ET. The corresponding correlation of the τ_d values from Table 5 (Figure 11) yields the k_Q value of 1.21×10^9 M^{-1} s^{-1}, which means that, at typically mM TRIR concentrations, the bimolecular rate will be on the order of 10^6 s^{-1}. Therefore, the maximum contribution of the bimolecular reaction to the reported ET rates is ~10%, comparable to the experimental error. We can thus conclude that the reported kinetics are predominantly due to the intramolecular ET pathway, shown by the red arrows in Scheme 1. For emission experiments, the bimolecular contribution will be about 10 times smaller because of lower concentrations. The BET rate constant is concentration-independent (Table 5), in accordance with the conclusion that most of the ET occurs intramolecularly.

DISCUSSION

Rhenium(I) carbonyl-diimine complexes with appended tryptophan undergo photoinduced electron transfer from the Trp(indole) group to the MLCT-excited Re chromophore, followed

Scheme 2. Intramolecular Photoinduced Electron Transfer in $[Re^I(L\text{-}Trp)(CO)_3(bpy)]^+$ [a]

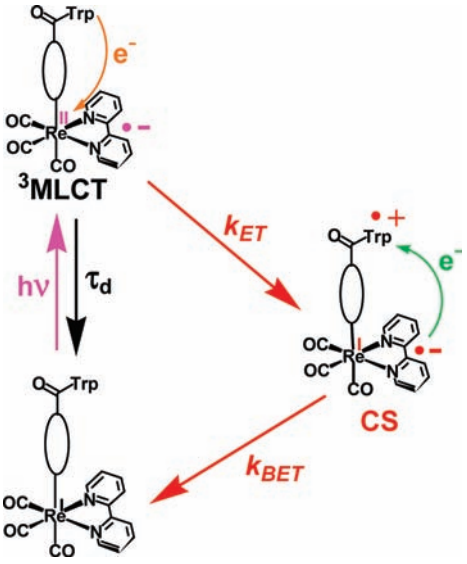

[a] The forward Trp(indole)→*Re^{II} and back $bpy^{\bullet-}$→$Trp(indole^{\bullet+})$ ET steps are indicated by orange and green arrows, respectively.

by the corresponding back-ET (Scheme 1). ET proceeds both intra- and intermolecularly, the former pathway being predominant. The intermolecular quenching contributing no more than 10% to the reaction rate, we will discuss the kinetics parameters from the intramolecular point of view (Scheme 2).

The MLCT excited state exhibits a ν(CO) IR spectrum that is typical of MLCT states in cationic Re complexes[11,29,40,55,57,65,66] such as $[Re(Etpy)(CO)_3(N,N)]^+$ or analogous $[Re(L\text{-}Phe/L\text{-}Tyr)(CO)_3(N,N)]^+$. These observations exclude any significant contribution from indole→N,N CT to the reactive excited state that would be manifested[11] by the shift of the A′(1) ν(CO) band upon excitation of about +10 cm^{-1} instead of the observed 37 (bpy) or 26 cm^{-1} (phen). Nevertheless, the indole group exerts some influence on the MLCT excited-state energy, as is documented by small blue shifts of the emission band on going from nicphe to nictrp and imphe to imtrp complexes (Supporting Information, Figure S2). Despite being predominantly localized at the $Re(CO)_3(N,N)$ chromophore, MLCT excitation shifts the amide-I vibration by ca. +9 cm^{-1} (Figure 8), demonstrating that the amide bridging group and the excited $Re(CO)_3(N,N)$ chromophore are electronically coupled.

The Trp(indole)→*Re^{II} ET occurs with a driving force of about 0.2 V,[67] in the Marcus normal region. The slightly faster rate in phen than bpy complexes (Table 2) could be due to ~0.14 eV higher driving force.[40,67] The observed increase of the ET rate with decreasing solvent dielectric function (Table 3), caused by decreasing outer-sphere reorganization energy λ_o, is expected for a nonadiabatic reaction.[68] The relatively slow ET rates, in the $(\sim 30\ ns)^{-1}$ range, are in agreement with the absence of a direct contact between the Trp(indole) and the $Re(CO)_3(N,N)$ chromophore. For comparison, a much faster (~500 ps) Trp(indole)→*Re^{II} ET has been observed[10] in a Re-labeled azurin mutant Re124W122Az containing a Trp residue placed next to the Re^I(histidine)(CO_3)(4,7-Me_2-phen) label. The fast ET in this case is attributable[10,11] to an indole−phen $\pi-\pi$ stacking, proven crystallographically. Picosecond ET to the MLCT-excited

dx.doi.org/10.1021/ic200252z |Inorg. Chem. 2011, 50, 6122–6134

Re^{I} chromophore also was observed in a chromophore−quencher complex $[Re(py\text{-}CH_2\text{-}PTZ)(CO)_3(bpy)]^+$ (PTZ = phenothiazine)[69] with a short bent $-CH_2-$ linker, and $[Re(py\text{-}azacrown)(CO)_3(bpy)]^+$, where the electron-donating azacrown N-atom is linked to the pyridine ligand through a −N(H)−C(=O)−ph− bridge.[70]

The photoinduced ET in $[Re^{I}(L\text{-}Trp)(CO)_3(N,N)]^+$ can occur either through space, mediated by intervening solvent molecules, or through σ bonds.[9,71,72] The former looks unlikely since both NMR and DFT indicate that the Trp(indole) donor group in the most stable conformation points away from the $Re(CO)_3(N,N)$ chromophore. However, the L-Trp ligands are flexible, and conformational movements may influence the electronic coupling[7] by changing the bond angles and the Re−indole distance. Therefore, the Trp(indole)→$*Re^{II}$ ET could be gated by fluctuations of solvated tryptophan whereby through-space ET would occur (ultra)fast, but only in favorable structural arrangements. However, there is no experimental evidence for this proposition so far. On the other hand, the through-bond mechanism is supported by the observed 4-fold ET acceleration on going from pytrp to nictrp complexes, i.e., upon shortening the ET path by one C−C bond.[73]

The CS state $[Re^{I}(L\text{-}Trp^{\bullet+})(CO)_3(N,N^{\bullet-})]^+$ is analogous to interligand CT states observed in Re-based chromophore−quencher complexes.[61,69,70] The CS term is preferred in the context of L-Trp complexes because the interaction between the two redox centers is rather weak. The oxidized tryptophan moiety is assumed to be in the protonated form ($Trp^{\bullet+}$) for two reasons: (i) no proton acceptor is present in the system, and (ii) $Trp^{\bullet+}$ deprotonation is slower (∼130 ns in H_2O)[20] than the CS-state decay. The absence of a suitable proton acceptor also explains why a Tyr→$*Re^{II}$ ET does not take place upon irradiation of the tyrosine complex $[Re^{I}(pytyr)(CO)_3(bpy)]^+$: The $Tyr^{\bullet+}$/Tyr potential is higher than +1.35 V (vs NHE),[74] apparently above the $*Re^{II}/Re^{I}$ excited-state potential of about 1.2−1.3 V,[67] making the ET thermodynamically unfavorable. On the other hand, Tyr photooxidation has been observed in $[Re^{I}(Ph_2P-ph-Tyr)(CO)_3(phen)]^+$ even at acidic pH due to a much higher $*Re^{II}/Re^{I}$ potential, +1.78 V.[16]

The BET rate does not show any systematic dependence on the L-Trp and N,N ligands or the solvent, although it is slightly faster for nictrp than pytrp. BET is a highly inverted process, occurring with a 2.0−2.2 eV driving force.[67] The observed BET rates (Table 2) are comparable to those reported for more strongly coupled $[Re(py\text{-}CH_2\text{-}PTZ)(CO)_3(bpy)]^+$ and $[Re(py\text{-}azacrown)(CO)_3(bpy)]^+$, 4×10^7 and 5.3×10^7 s^{-1}, respectively,[69,70] as well as for the Re-labeled azurin mutant Re124W122Az, 2×10^7 s^{-1}.[10] The fast BET rates in $[Re(L\text{-}Trp)(CO)_3(N,N)]^+$ suggest the possibility of a through-space interaction in the CS state between the negatively charged diimine and positively charged indole rings. Emergence of such an interaction would require a conformational change of the CS state, whose occurrence seems to be manifested by the small shift and a shape change of the IR band 5 on a tens of nanoseconds time scale. Moreover, the TRIR behavior in the region of the amide-I band (Figure 8) suggests that the amide bridge geometry changes on going from the MLCT to the CS state.

In conclusion, we have demonstrated intramolecular photooxidation of tryptophan (but not tyrosine) by appended $Re^{I}(CO)_3(N,N)$ chromophores in a variety of aprotic solvents that occurs with a lifetime of 8−40 ns. A ligand-appended tryptophan radical−cation is generated in a sufficient concentration to study its spectroscopic properties and reactivity, limited only by the 30−60 ns back-electron-transfer. The $[Re(L\text{-}Trp^{\bullet+})(CO)_3(N,N^{\bullet-})]^+$ transient yield can be maximized by (i) prolonging the inherent MLCT lifetime (τ_0) by using phen instead of bpy and linking Trp to Re through pyridine instead of imidazole, (ii) maximizing the forward ET rate either by ligand engineering (nictrp is superior to pytrp and imtrp) or using nonpolar solvents with small dielectric functions, and (iii) minimizing the back-ET rate that, however, appears to be the least tunable factor. The present study also independently demonstrates the feasibility of Trp to act as an electron-hopping intermediate in Re-labeled proteins and photodriven supramolecular ET systems.

■ ASSOCIATED CONTENT

Supporting Information. UV−vis absorption spectra of $[Re(L\text{-}AA)(CO)_3(bpy)]^+$, emission spectra of $[Re(L\text{-}AA)(CO)_3(N,N)]^+$, emission decay profiles of $[Re(L\text{-}AA)(CO)_3(bpy)]^+$ and their emission-wavelength dependences, TRIR spectra of $[Re(pytrp)(CO)_3(bpy)]^+$ in DMF, transient lifetimes of $[Re(pyphe)(CO)_3(bpy)]^+$ and $[Re(pytrp)(CO)_3(bpy)]^+$ as a function of solvent, and the full reference for the Gaussian 2009 software. This material is available free of charge via the Internet at http://pubs.acs.org.

■ AUTHOR INFORMATION

Corresponding Author
*E-mail: a.vlcek@qmul.ac.uk.

■ ACKNOWLEDGMENT

This research was supported by STFC Rutherford Appleton Laboratory (CMSD 43), QMUL, European collaboration program COST D35, and the Czech Ministry of Education grant LD11082. Dr. H. Toms and Prof. G. E. Hawkes (QMUL) are thanked for measuring and interpreting the ^1H NOESY spectra.

■ REFERENCES

(1) Byrdin, M.; Eker, A. P. M.; Vos, M. H.; Brettel, K. *Proc. Natl. Acad. Sci. U. S. A.* **2003**, *100*, 8676–8681.
(2) Lukacs, A.; Eker, A. P. M.; Byrdin, M.; Brettel, K.; Vos, M. H. *J. Am. Chem. Soc.* **2008**, *130*, 14394.
(3) Byrdin, M.; Lukacs, A.; Thiagarajan, V.; Eker, A. P. M.; Brettel, K.; Vos, M. H. *J. Phys. Chem. A* **2010**, *114*, 3207–3214.
(4) Stubbe, J.; Nocera, D. G.; Yee, C. S.; Chang, M. C. Y. *Chem. Rev.* **2003**, *103*, 2167.
(5) Reece, S. Y.; Hodgkiss, J. M.; Stubbe, J.; Nocera, D. G. *Philos. Trans. R. Soc. B* **2006**, *361*, 1351.
(6) Loll, B.; Kern, J.; Saenger, W.; Zouni, A.; Jacek Biesiadka, J. *Nature* **2005**, *438*, 1040.
(7) Gray, H. B.; Winkler, J. R. *Chem. Phys. Lett.* **2009**, *483*, 1.
(8) Winkler, J. R.; Di Bilio, A. J.; Farrow, N. A.; Richards, J. H.; Gray, H. B. *Pure Appl. Chem.* **1999**, *71*, 1753.
(9) Gray, H. B.; Winkler, J. R. *Proc. Natl. Acad. Sci. U.S.A.* **2005**, *102*, 3534.
(10) Shih, C.; Museth, A. K.; Abrahamsson, M.; Blanco-Rodriguez, A. M.; Di Bilio, A. J.; Sudhamsu, J.; Crane, B. R.; Ronayne, K. L.; Towrie, M.; Vlček, A., Jr.; Richards, J. H.; Winkler, J. R.; Gray, H. B. *Science* **2008**, *320*, 1760.
(11) Blanco-Rodríguez, A. M.; Di Bilio, A. J.; Shih, C.; Museth, A. K.; Clark, I. P.; Towrie, M.; Cannizzo, A.; Sudhamsu, J.; Crane, B. R.; Sýkora, J.; Winkler, J. R.; Gray, H. B.; Záliš, S.; Vlček, A., Jr. *Chem.—Eur. J.* **2011**, *17*, 5350–5361.

(12) Reece, S. Y.; Seyedsayamdost, M. R.; Stubbe, J.; Nocera, D. G. *J. Am. Chem. Soc.* **2007**, *129*, 13828.
(13) Vlček, A., Jr. *Top. Organomet. Chem.* **2010**, *29*, 73.
(14) Kumar, A.; Sun, S.-S.; Lees, A. J. *Top. Organomet. Chem.* **2010**, *29*, 1.
(15) Pan, J.; Xu, Y.; Benkö, G.; Feyziyev, Y.; Styring, S.; Sun, L.; Åkermark, B.; Polívka, T.; Sundström, V. *J. Phys. Chem. B* **2004**, *108*, 12904.
(16) Reece, S. Y.; Nocera, D. G. *J. Am. Chem. Soc.* **2005**, *127*, 9448.
(17) Reece, S. Y.; Seyedsayamdost, M. R.; Stubbe, J.; Nocera, D. G. *J. Am. Chem. Soc.* **2006**, *128*, 13654.
(18) Ishikita, H.; Alexander V. Soudackov, A. V.; Hammes-Schiffer, S. *J. Am. Chem. Soc.* **2007**, *129*, 11146.
(19) Sjödin, M.; Styring, S.; Åkermark, B.; Sun, L.; Hammarström, L. *J. Am. Chem. Soc.* **2000**, *122*, 3932.
(20) Sjödin, M.; Styring, S.; Wolpher, H.; Xu, Y.; Sun, L.; Hammarström, L. *J. Am. Chem. Soc.* **2005**, *127*, 3855.
(21) Irebo, T.; Johansson, O.; Leif Hammarström, L. *J. Am. Chem. Soc.* **2008**, *130*, 9194.
(22) Lo, K. K.-W.; Tsang, K. H.-K.; Hui, W.-K.; Zhu, N. *Inorg. Chem.* **2005**, *44*, 6100.
(23) Lo, K. K.-W.; Lee, T. K.-M.; Zhang, K. Y. *Inorg. Chim. Acta* **2006**, *359*, 1845–1854.
(24) Lo, K. K.-W.; Sze, K.-S.; Tsang, K. H.-K.; Zhu, N. *Organometallics* **2007**, *26*, 3440.
(25) Lo, K. K.-W.; Louie, M.-W.; Zhang, K. Y. *Coord. Chem. Rev.* **2010**, *254*, 2603–2622.
(26) Hino, J. K.; Della Ciana, L.; Dressick, W. J.; Sullivan, B. P. *Inorg. Chem.* **1992**, *31*, 1072.
(27) Towrie, M.; Grills, D. C.; Dyer, J.; Weinstein, J. A.; Matousek, P.; Barton, R.; Bailey, P. D.; Subramaniam, N.; Kwok, W. M.; Ma, C. S.; Phillips, D.; Parker, A. W.; George, M. W. *Appl. Spectrosc.* **2003**, *57*, 367.
(28) Vlček, A., Jr.; Farrell, I. R.; Liard, D. J.; Matousek, P.; Towrie, M.; Parker, A. W.; Grills, D. C.; George, M. W. *J. Chem. Soc., Dalton Trans.* **2002**, 701.
(29) Blanco-Rodríguez, A. M.; Ronayne, K. L.; Záliš, S.; Sýkora, J.; Hof, M.; Vlček, A., Jr. *J. Phys. Chem. A* **2008**, *112*, 3506.
(30) Towrie, M.; Parker, A. W.; Vlček, A., Jr.; Gabrielsson, A.; Blanco Rodriguez, A. M. *Appl. Spectrosc.* **2005**, *59*, 467.
(31) Greetham, G.; Burgos, P.; Cao, Q.; Clark, I. P.; Codd, P.; Farrow, R.; George, M. W.; Kogimtzis, M.; Matousek, P.; Parker, A. W.; Pollard, M.; Robinson, D.; Xin, Z.-J.; Towrie, M. *Appl. Spectrosc.* **2010**, *64*, 1311.
(32) Frisch, M. J. et al. *Gaussian 09, Revision A.02*; Gaussian, Inc.: Wallingford CT, 2009.
(33) Perdew, J. P.; Burke, K.; Ernzerhof, M. *Phys. Rev. Lett.* **1996**, *77*, 3865.
(34) Adamo, C.; Barone, V. *J. Chem. Phys.* **1999**, *110*, 6158.
(35) Yanai, T.; Tew, D. P.; Handy, N. C. *Chem. Phys. Lett.* **2004**, *393*, 51.
(36) Raghavachari, K.; Binkley, J. S.; Seeger, R.; Pople, J. A. *J. Chem. Phys.* **1980**, *72*, 650.
(37) Andrae, D.; Häussermann, U.; Dolg, M.; Stoll, H.; Preuss, H. *Theor. Chim. Acta* **1990**, *77*, 123.
(38) Martin, J. M. L.; Sundermann, A. *J. Chem. Phys.* **2001**, *114*, 3408.
(39) Tomasi, J.; Mennucci, B.; Cammi, R. *Chem. Rev.* **2005**, *105*, 2999.
(40) Dattelbaum, D. M.; Omberg, K. M.; Schoonover, J. R.; Martin, R. L.; Meyer, T. J. *Inorg. Chem.* **2002**, *41*, 6071.
(41) Stufkens, D. J.; Vlček, A., Jr. *Coord. Chem. Rev.* **1998**, *177*, 127.
(42) Horng, M. L.; Gardecki, J. A.; Papazyan, A.; Maroncelli, M. *J. Phys. Chem.* **1995**, *99*, 17311.
(43) Záliš, S.; Consani, C.; El Nahhas, A.; Cannizzo, A.; Chergui, M.; Hartl, F.; Vlček, A.Jr.; *Inorg. Chim. Acta* **2011**, in press, doi:10.1016/j.ica.2011.02.084.
(44) Kalyanasundaram, K. *J. Chem. Soc. Faraday Trans. 2* **1986**, *82*, 2401.
(45) El Nahhas, A.; Cannizzo, A.; van Mourik, F.; Blanco-Rodríguez, A. M.; Záliš, S.; Vlček, A., Jr.; Chergui, M. *J. Phys. Chem. A* **2010**, *114*, 6361.
(46) El Nahhas, A.; Consani, C.; Blanco-Rodríguez, A. M.; Lancaster, K. M.; Braem, O.; Cannizzo, A.; Towrie, M.; Clark, I. P.; Záliš, S.; Chergui, M.; Vlček, A., Jr. *Inorg. Chem.* **2011**, *50*, 2932–2943.
(47) George, M. W.; Johnson, F. P. A.; Westwell, J. R.; Hodges, P. M.; Turner, J. J. *J. Chem. Soc., Dalton Trans.* **1993**, 2977.
(48) Gamelin, D. R.; George, M. W.; Glyn, P.; Grevels, F.-W.; Johnson, F. P. A.; Klotzbücher, W.; Morrison, S. L.; Russell, G.; Schaffner, K.; Turner, J. J. *Inorg. Chem.* **1994**, *33*, 3246.
(49) Dattelbaum, D. M.; Omberg, K. M.; Hay, P. J.; Gebhart, N. L.; Martin, R. L.; Schoonover, J. R.; Meyer, T. J. *J. Phys. Chem. A* **2004**, *108*, 3527.
(50) Dattelbaum, D. M.; Martin, R. L.; Schoonover, J. R.; Meyer, T. J. *J. Phys. Chem. A* **2004**, *108*, 3518.
(51) Vlček, A., Jr.; Záliš, S. *Coord. Chem. Rev.* **2007**, *251*, 258.
(52) Asbury, J. B.; Wang, Y.; Lian, T. *Bull. Chem. Soc. Jpn.* **2002**, *75*, 973.
(53) Lenchenkov, V. A.; She, C.; Lian, T. *J. Phys. Chem. B* **2004**, *108*, 16194.
(54) Liard, D. J.; Busby, M.; Matousek, P.; Towrie, M.; Vlček, A., Jr. *J. Phys. Chem. A* **2004**, *108*, 2363.
(55) Blanco-Rodríguez, A. M.; Busby, M.; Grădinaru, C.; Crane, B. R.; Di Bilio, A. J.; Matousek, P.; Towrie, M.; Leigh, B. S.; Richards, J. H.; Vlček, A., Jr.; Gray, H. B. *J. Am. Chem. Soc.* **2006**, *128*, 4365.
(56) Blanco-Rodríguez, A. M.; Towrie, M.; Collin, J.-P.; Záliš, S.; Vlček, A., Jr. *Dalton Trans.* **2009**, 3941.
(57) Blanco-Rodríguez, A. M.; Busby, M.; Ronayne, K. L.; Towrie, M.; Sýkora, J.; Hof, M.; Záliš, S.; Grădinaru, C.; Di Bilio, A. J.; Crane, B. R.; Gray, H. B.; Vlček, J., A. *J. Am. Chem. Soc.* **2009**, *131*, 11788.
(58) Johnson, F. P. A.; George, M. W.; Hartl, F.; Turner, J. J. *Organometallics* **1996**, *15*, 3374.
(59) Gabrielsson, A.; Hartl, F.; Zhang, H.; Lindsay Smith, J. R.; Towrie, M.; Vlček, A., Jr.; Perutz, R. N. *J. Am. Chem. Soc.* **2006**, *128*, 4253.
(60) Stor, G. J.; Hartl, F.; van Outersterp, J. W. M.; Stufkens, D. J. *Organometallics* **1995**, *14*, 1115.
(61) Lewis, J. D.; Towrie, M.; Moore, J. N. *J. Phys. Chem. A* **2008**, *112*, 3852.
(62) Omberg, K. M.; Schoonover, J. R.; Treadway, J. A.; Leasure, R. M.; Dyer, R. B.; Meyer, T. J. *J. Am. Chem. Soc.* **1997**, *119*, 7013.
(63) Liard, D. J.; Busby, M.; Farrell, I. R.; Matousek, P.; Towrie, M.; Vlček, A., Jr. *J. Phys. Chem. A* **2004**, *108*, 556.
(64) *Handbook of Chemistry and Physics*; CRC Press: Boca Raton, FL, 2002.
(65) Gabrielsson, A.; Matousek, P.; Towrie, M.; Hartl, F.; Záliš, S.; Vlček, A., Jr. *J. Phys. Chem. A* **2005**, *109*, 6147.
(66) Busby, M.; Matousek, P.; Towrie, M.; Clark, I. P.; Motevalli, M.; Hartl, F.; Vlček, A., Jr. *Inorg. Chem.* **2004**, *43*, 4523.
(67) The driving force of the forward reaction is estimated as $^*E(Re^{II}/Re^{I}) - E^o(Trp^{\bullet+}/Trp)$, where the excited-state potential $^*E(Re^{II}/Re^{I}) \cong E_{00} - E^o(N,N/N,N^{\bullet-})$. A value of +1.1 V (vs NHE) is assumed for $E^o(Trp^{\bullet+}/Trp)$.[74,75] The reduction potentials and excited-state energy E_{00} of pytrp and nictrp complexes are assumed to be similar to those of the corresponding $[Re(Etpy)(CO)_3(N,N)]^+$ complexes[40], giving $^*E(Re^{II}/Re^{I})$ of +1.29 and +1.48 V for N,N = bpy and phen, respectively. Reduction of $[Re(im)(CO)_3(bpy)]^+$ is expected (by analogy with the phen complex[76]) to be slightly more negative while emission occurs at lower energies than in the pytrp and nictrp complexes. Hence, we estimate the $^*E(Re^{II}/Re^{I})$ potential of $[Re(imtrp)(CO)_3(bpy)]^+$ as +1.2 V. The BET driving force is estimated as $E^o(Trp^{\bullet+}/Trp) + E^o(N,N/N,N^{\bullet-})$.
(68) Marcus, R. A.; Sutin, N. *Biochim. Biophys. Acta* **1985**, *811*, 265.
(69) Chen, P.; Westmoreland, T. D.; Danielson, E.; Schanze, K. S.; Anthon, D.; Neveux, P. E., Jr.; Meyer, T. J. *Inorg. Chem.* **1987**, *26*, 1116.
(70) Lewis, J. D.; Bussotti, L.; Foggi, P.; Perutz, R. N.; Moore, J. N. *J. Phys. Phem. A* **2002**, *106*, 12202.
(71) Wenger, O. S.; Leigh, B. S.; Villahermosa, R. M.; Gray, H. B.; Winkler, J. R. *Science* **2005**, *307*, 99.
(72) Kaplan, R.; Napper, A. M.; Waldeck, D. H.; Zimmt, M. B. *J. Phys. Chem. A* **2002**, *106*, 1917.

(73) This argument seems to be countered by ET in $[Re(imtrp)(CO)_3(bpy)]^+$ being slower than in $[Re(nictrp)(CO)_3(bpy)]^+$, despite involving the same number of σ bonds. However, this difference could be caused by at least ~50 mV smaller driving force in $[Re(imtrp)(CO)_3(bpy)]^+$.

(74) Tommos, C.; Skalicky, J. J.; Pilloud, D. L.; Wand, A. J.; Dutton, P. L. *Biochemistry* **1999**, *38*, 9495.

(75) Harriman, A. *J. Phys. Chem.* **1987**, *91*, 6102.

(76) Connick, W. B.; Di Bilio, A. J.; Hill, M. G.; Winkler, J. R.; Gray, H. B. *Inorg. Chim. Acta* **1995**, *240*, 169.